Chapter in a book, "Raman Scattering in Solids", Springer-Verlag (Germany), Manuel Cardona, Ed.

LBL-2709
Preprint

STIMULATED RAMAN SCATTERING

Y. R. Shen

March 1974

Prepared for the U. S. Atomic Energy Commission
under Contract W-7405-ENG-48

LBL-2709

DISCLAIMER

LBL-2709

Stimulated Raman Scattering

Y. R. Shen

Department of Physics, University of California, Berkeley
and
Inorganic Materials Research Division,
Lawrence Berkeley Laboratory,
Berkeley, California 94720

S1.1 INTRODUCTION

It is well known that Raman scattering is a direct two-photon process. Simultaneously in the process, one photon at $\omega_1(\vec{k}_1)$ is absorbed and one photon at $\omega_2(\vec{k}_2)$ is emitted while the material makes a transition from the initial state $|i\rangle$ to the final state $|f\rangle$ (see Fig. S.1). Energy conservation requires $\hbar(\omega_1-\omega_2)$ to be equal to the energy difference of the two states $E_f - E_i = \hbar\omega_{fi}$ within the uncertainty limit of the linewidth. We can have either $\omega_1 > \omega_2$ or $\omega_1 < \omega_2$. The former is known as Stokes scattering and the latter antiStokes scattering.

A straightforward second-order perturbation calculation leads to the following Raman transition probability per unit time per unit volume per unit energy interval [S.1]

$$\frac{dW_{fi}}{d(\hbar\omega)} = (8\pi^3 N\omega_1\omega_2/\varepsilon_1\varepsilon_2)\,|\langle f|M|i\rangle|^2\langle\alpha_f|a_2^+a_1|\alpha_i\rangle|^2 g(\Delta\omega)$$

$$M = \frac{e^2}{m^2\omega_1\omega_2}\sum_s\left\{\frac{e^{-i\vec{k}_2\cdot\vec{r}}(\vec{p}\cdot\hat{e}_2)\,|s\rangle\langle s|\,(\vec{p}\cdot\hat{e}_1)e^{i\vec{k}_1\cdot\vec{r}}}{\hbar(\omega_1-\omega_{si})}\right.$$

$$\left. - \frac{(\vec{p}\cdot\hat{e}_1)e^{i\vec{k}_1\cdot\vec{r}}\,|s\rangle\langle s|\,e^{-i\vec{k}_2\cdot\vec{r}}(\vec{p}\cdot\hat{e}_2)}{\hbar(\omega_2+\omega_{si})}\right\}. \qquad \text{(S-1)}$$

Here, N is the density of molecules or unit cells in the medium, ε is the dielectric constant, $\vec{p}$ is the momentum operator, $\hat{e}$ denotes the field polarization, $|s\rangle$ is the intermediate state of the material system, $|\alpha\rangle$ denotes the state of the radiation field, a^+ and a are the photon creation and annihilation operators respectively, and finally g ($\Delta\omega \equiv \omega_1-\omega_2-\omega_{fi}$) is the joint density of states of the transition. If the Raman transition has a Lorentzian lineshape, then $g(\Delta\omega) = \Gamma/\pi[(\Delta\omega)^2+\Gamma^2]$

where Γ is the halfwidth of the line.

The transition probability W_{fi} in Eq. (S-1) is proportional to $|\langle\alpha_f|a_2^+a_1|\alpha_i\rangle|^2$. If the Raman process begins with an initial state which contains practically no photon at ω_2, it is known as spontaneous Raman emission. Then, W_{fi} is simply proportional to $|\langle\alpha_f|a_1|\alpha_i\rangle|^2$. Otherwise, it is known as stimulated Raman emission. In the particular case where the states contain integer numbers of photons at ω_1 and ω_2 such that $|\alpha_i\rangle = |n_1,n_2\rangle$ and $|\alpha_f\rangle = |n_1-1, n_2+1\rangle$, we have $W_{fi} \propto n_1(n_2+1)$; spontaneous Raman scattering corresponds to $n_2 = 0$ in this case. In general, the radiation states are more complex [S-2], and no such simple relation can be obtained. However, if the average numbers of photons $\bar{n}_1$ and $\bar{n}_2$ at ω_1 and ω_2 are much larger than 1, then the approximation $|\langle\alpha_f|a_2^+a_1|\alpha_i\rangle|^2 \cong \bar{n}_1\bar{n}_2$ is excellent [S.2].

Thus, we expect that the spontaneous Raman scattering cross-section should be linearly proportional to the stimulated Raman gain coefficient. By definition, the differential Raman cross-section $d^2\sigma/d(\hbar\omega_2)d\Omega$ is the probability of a unit volume of material scattering an incident photon at ω_1 per unit area into a Raman photon of one polarization at ω_2 in a unit solid angle around Ω and a unit energy interval around $\hbar\omega_2$. Since the density of radiation modes per unit solid angle is $g_E d\omega_2 = k_2^2 dk_2/(2\pi)^3$, we have

$$d^2\sigma/d(\hbar\omega_2)d\Omega = \rho_i g_E[dW_{fi}/d(\hbar\omega_2)]/|\langle\alpha_f|a_2^+a_1|\alpha_i\rangle|^2_c$$

$$= N\frac{\omega_1\omega_2^3\varepsilon_2^{1/2}}{c^4\varepsilon_1}|M_{fi}|^2 g(\Delta\omega)\rho_i \qquad \text{(S-2)}$$

where $M_{fi} = \langle f|M|i \rangle$ and ρ_i is the population of $|i\rangle$. In the stimulated Raman amplification, the change of the number of Raman photons in one mode per unit length of propagation is given by [S.3]

$$\frac{d\bar{n}_2}{dz} = \left(\frac{dW_{fi}}{d\omega_2}\rho_i - \frac{dW_{if}}{d\omega_2}\rho_f\right)\varepsilon_2^{1/2}/c - \alpha_2\bar{n}_2 \qquad \text{(S-3a)}$$

$$\cong (G_R - \alpha_2)\bar{n}_2 \qquad \text{if } \bar{n}_1, \bar{n}_2 \gg 1 \qquad \text{(S-3b)}$$

$$G_R = 8\pi^3 N\hbar(\omega_1\omega_2/\varepsilon_1\varepsilon_2)|M_{fi}|^2 g(\Delta\omega)(\rho_i - \rho_f)\bar{n}_1(\varepsilon_2^{1/2}/c)$$

$$= \frac{4\pi^2 c^3 \varepsilon_1}{\omega_1\omega_2^2\varepsilon_2\rho_i}(\rho_i - \rho_f)\left(\frac{d^2\sigma}{d(\hbar\omega_2)d\Omega}\right)|E_1|^2$$

where α_2 is the absorption coefficient at ω_2, and $|E_1|^2\eta_1^2/2\pi = \bar{n}_1\hbar\omega$ is the field energy per unit volume. Equation (S-3) shows that G_R is the Raman gain and is proportional to $d^2\sigma/d(\hbar\omega_2)d\Omega$. In the next section, we shall show that we can obtain the same expression for G_R from a third-order nonlinear optical susceptibility, known as the Raman susceptibility.

In Table I, we list a number of Raman lines for some of the materials in which both spontaneous and stimulated Raman scattering have been measured. Note that the material which has the strongest Raman gain is InSb. From Eq. (S-3), we have $n_2(\ell) = n_2(0)\exp[(G_R - \alpha_2)\ell]$. Then, even in InSb, in order to generate e^{30} Raman photons from one noise photon in a 1-cm crystal, we need an incident CO_2 laser intensity of 2 MW/cm^2. For this reason, stimulated Raman scattering was only observed after the high-power laser was invented.

Stimulated Raman scattering was accidentally discovered by Woodburg and Ng in 1962 [S.4]. In studying Q-switching of a ruby laser by a nitrobenzene Kerr cell, they detected intense infrared radiation emitted from the Kerr cell. Hellwarth [S.3] soon correctly pointed out that the infrared radiation came from stimulated Raman emission. Subsequently, similar effect was observed in many other liquids by Eckhardt et al. [S.5], Geller et al. [S.6], and Stoicheff [S.7], in several solids by Eckhardt et al. [S.8], and in hydrogen gas by Minck et al. [S.9].

As seen from Table I, one would need a laser beam of 1 GW/cm^2 propagating over a 15-cm nitrobenzene cell in order to generate e^{30} Raman photons from a noise photon. These numbers are roughly the same for many other liquids from which stimulated Raman emission has been observed. However, in the earlier experiments on stimulated Raman scattering, laser beams of less than 100 MW/cm^2 were used, yet more than e^{30} Raman photons per sec were recorded. This anomaly, together with a number of other observed anomalies [S.7] such as the extremely sharp stimulated Raman threshold, the asymmetry of forward-backward Raman intensity, the appreciable spectral broadening of the Raman radiation, etc., has baffled research workers in the field for quite a few years. As we shall see in a later section, these anomalies are now understood as due to self-focusing of the incident laser beam in the medium.

Both Stokes and antiStokes radiation are normally observed in stimulated Raman scattering. The observation of stimulated antiStokes scattering [S.10] was quite surprising since from the simple theory of two-photon transitions as described by Eq. (S-3), the antiStokes Raman gain is negative with $\omega_1 - \omega_2 \approx \omega_{fi} < 0$ and $\rho_i < \rho_f$ at thermal equilibrium.

We shall see later that the antiStokes radiation is actually generated through parametric coupling with the laser and Stokes radiation. This also explains why the antiStokes generated in liquids and solids always has intense components radiated in the off-axis directions.

Higher-order Stokes and antiStokes radiation are also frequently observed [S.10-12]. They are presumably generated by stepwise processes. Because of high laser intensity in the medium (usually in local region through either external focusing or self-focusing), intense first-order Stokes and antiStokes radiation are first generated. They are then intense enough to generate second-order Raman radiation which in turn may become intense enough to generate higher-order Raman radiation. The theoretical description of this stepwise Raman production is however very difficult, as we shall see.

Early interest in stimulated Raman scattering arose because it can provide intense coherent radiation at new frequencies and because it is a possible loss mechanism in transmitting high-power laser beams through a medium, for example, the atmosphere. Later, it was demonstrated that stimulated Raman scattering via phonons which are both Raman and infrared active can have its Raman frequency tuned continuously over a certain range by varying the directions of the beam propagation in a crystal [S.13]. This is known as stimulated polariton scattering. Tunable far-infrared radiation at $(\omega_1-\omega_2)$ is generated simultaneously with the Raman radiation in stimulated polariton scattering [S.14]. Then, it was discovered that stimulated Raman scattering can also occur via two-photon spin-flip transitions in semiconductors (observed in InSb) [S.15]. The Raman frequency is again continuously tunable by adjusting the Zeeman splitting

with an applied magnetic field. Since the spin-flip transitions can also be induced directly by far-infrared radiation, the problem is rather similar to the problem of stimulated polariton scattering. We can in fact use the theory of stimulated polariton scattering to correctly describe both stimulated Raman emission and far-infrared generation via spin-flip transitions in InSb [S.16].

The relaxation times of the Raman effect in liquids and solids are usually very short, in the picosecond range. Therefore, with nanosecond incident laser pulses, the Raman generation (in the absence of self-focusing) can certainly be regarded as quasi-steady-state. But when picosecond laser pulses are used, the transient effect in the Raman generation may become important [S.17]. The theory of transient stimulated Raman scattering is now well understood [S.18]. Experimentally, the transient Raman effect has been used to excite coherent molecular or phonon vibration in a medium. By monitoring the decay of such a forced vibration, one can then measure the corresponding vibrational relaxation times [S.19,20]. So far, this has been the only existing method for measuring vibrational relaxation times of liquids and solids directly.

In Section II, we shall discuss the classical theory of stimulated Raman scattering. We shall use the coupled wave approach [S.21] to describe the generation of first- and higher-order Stokes and antiStokes radiation [S.22]. In Section III, we shall review the experimental results on stimulated Raman effect and show how we can explain the various anomalous effects observed in stimulated Raman scattering. In Sections IV and V, we shall discuss two special cases of stimulated Raman scattering, namely, stimulated polariton scattering and stimulated spin-flip Raman emission. In Section VI, we shall consider the transient behavior of stimulated Raman emission when the pulsewidth of the pump field is either narrower than, or comparable with the relaxation times of the Raman excitation. In Section VII, we shall discuss a number of possible applications of stimulated Raman scattering. These include measurements of phonon or vibrational relaxation times, measurements of third-order nonlinear refractive indices, detection of substances of low concentration, spectroscopic studies of low-energy excitations, heating of plasmas, and transmission of high-power laser beams in a medium. Finally, in Section VIII, we shall give brief concluding remarks on the anticipated future progress in this field.

There already exist in the literature several review articles on the stimulated Raman effect [S.23,24]. In this paper, we shall put more emphasis on the basic understanding of the effect and on the more recent progress in the field. The references quoted here are admittedly far from complete. For a more complete reference list, the readers should consult Refs. [S.23-24].

S1.2 THEORY OF STIMULATED RAMAN SCATTERING

We shall use only semiclassical descriptions in the following theoretical treatment of stimulated Raman scattering (SRS), i.e., we shall avoid quantization of electromagnetic fields. This is of course not valid when the number of phonons in the Raman mode is small, for example, when SRS is first initiated by the spontaneously scattered photons. Therefore, the descriptions are valid only for stimulated Raman amplification where the input Raman radiation is sufficiently intense. For Raman oscillation which builds up from spontaneous scattering, we must use the full quantum description, for example, Eq. (S-3a) with $W_{fi} \propto n_1(n_2+1)$ and $W_{if} \propto (n_1+1)n_2$. Sparks [S.25] has recently found a solution for stimulated Raman oscillation. There are numerous papers in the literature on the theory of SRS. See, for example, Refs. [S.3; S.26-30]. In this section, we shall discuss only the coupled-wave approach for stimulated Raman amplification [S.21,22].

S2.1 COUPLING OF PUMP AND STOKES WAVES

Consider the problem of SRS in a medium with energy levels shown in Fig. S.1. Let us first assume that only two frequency components, ω_1 and ω_2 with $\omega_1 > \omega_2$, are present (i.e., we consider only first-order Stokes scattering.) In the semiclassical description, these two components of the fields are represented by the waves

$$E_1 = \vec{\mathcal{E}}_1 \exp\,(i\vec{k}_1 \cdot \vec{r} - i\omega_1 t)$$

$$E_2 = \vec{\mathcal{E}}_2 \exp\,(i\vec{k}_2 \cdot \vec{r} - i\omega_2 t). \qquad \text{(S-4)}$$

In the steady-state case, they obey the wave equations

$$\nabla \times (\nabla \times \vec{E}_1) - \frac{\omega_1^2}{c^2} \overleftrightarrow{\varepsilon}_1 \cdot \vec{E}_1 = \frac{4\pi\omega_1^2}{c^2} \vec{P}^{(3)}(\omega_1)$$

$$\nabla \times (\nabla \times \vec{E}_2) - \frac{\omega_2^2}{c^2} \overleftrightarrow{\varepsilon}_2 \cdot \vec{E}_2 = \frac{4\pi\omega_2^2}{c^2} \vec{P}^{(3)}(\omega_2) \qquad \text{(S-5)}$$

where the nonlinear polarizations $\vec{P}^{NL}$ in a medium with inversion symmetry are given by [S.31]

$$\vec{P}^{(3)}(\omega_1) \cong (\chi_1^{(3)}|E_1|^2 + \chi_{R1}^{(3)}|E_2|^2)\vec{E}_1$$

$$\vec{P}^{(3)}(\omega_2) \cong (\chi_{R2}^{(3)}|E_1|^2 + \chi_2^{(3)}|E_2|^2)\vec{E}_2 \qquad \text{(S-6)}$$

where $\chi^{(3)}$ are third-order nonlinear susceptibilities.

We then see clearly that the two wave equations in Eq. (S-5) are actually coupled with each other through the $\chi_R^{(3)}$ terms in $\vec{P}^{(3)}$. This coupling between $\vec{E}_1$ and $\vec{E}_2$ causes effective energy transfer between the two waves. In this respect, $\chi_R^{(3)}$ are known as Raman susceptibilities. The $\chi_1^{(3)}$ and $\chi_2^{(3)}$ terms in $\vec{P}^{(3)}$ simply modify the dielectric constants $\varepsilon(\omega_1)$ and $\varepsilon(\omega_2)$ in Eq. (S-5). They are responsible for self-focusing of high-intensity beams with finite cross-sections. In the following, we shall, however, assume infinite plane wave propagation in the medium and hence we shall neglect $\chi_1^{(3)}$ and $\chi_2^{(3)}$.

Consider the waves propagating along $\hat{z}$. For cubic or isotropic media, $\nabla \times (\nabla \times \vec{E}) = -\partial^2\vec{E}/\partial z^2$. If the energy transfer between $\vec{E}_1$ and $\vec{E}_2$ is not so rapid that $\mathscr{E}_1$ and $\mathscr{E}_2$ can be considered as slowly varying functions

($|\partial^2\mathcal{E}/\partial z^2| \ll k|\partial\mathcal{E}/\partial z|$), then Eq. (S-5) reduces to

$$\partial\mathcal{E}_1/\partial z = i(2\pi\omega_1^2/c^2k_1)\chi_{R1}^{(3)}|E_2|^2\mathcal{E}_1$$

$$\partial\mathcal{E}_2/\partial z = i(2\pi\omega_2^2/c^2k_2)\chi_{R2}^{(3)}|E_1|^2\mathcal{E}_2 \qquad \text{(S-7)}$$

where $k = \omega\varepsilon^{1/2}/c$. From Eq. (S-7), we obtain

$$\partial|\mathcal{E}_1|^2/\partial z = -(4\pi\omega_1^2/c^2k_1)(\mathrm{Im}\chi_{R1}^{(3)})|\mathcal{E}_1|^2|\mathcal{E}_2|^2$$

$$\partial|\mathcal{E}_2|^2/\partial z = -(4\pi\omega_2^2/c^2k_1)(\mathrm{Im}\chi_R^{(3)})|\mathcal{E}_1|^2|\mathcal{E}_2|^2. \qquad \text{(S-8)}$$

We can now compare the second equation in Eq. (S-8) directly with Eq. (S-3), knowing $|\mathcal{E}_2|^2\varepsilon(\omega_1)/2\pi = \bar{n}_2\hbar\omega_2$. We then immediately find

$$G_R = -(4\pi\omega_2^2/c^2k_2)(I_m\chi_{R2}^{(3)})|\mathcal{E}_1|^2$$

$$\chi_{R2}^{(3)} = \frac{-c^4\varepsilon_1}{\omega_1\omega_2^3\varepsilon_2^{1/2}\rho_i}(\rho_i-\rho_f)\frac{1}{\hbar[(\omega_1-\omega_2-\omega_{fi})-i\Gamma]}\frac{d\sigma}{d\Omega} + (\chi_{R2}^{(3)})_{NR}. \qquad \text{(S-9)}$$

We assume here $g(\Delta\omega)$ is a Lorentzian and $(\chi_{R2}^{(3)})_{NR}$ is the non-resonant term due to non-resonant virtual transition. This yields a microscopic expression for $\chi_{R2}^{(3)}$

$$\chi_{R2}^{(3)} = -N|M_{fi}|^2(\rho_i-\rho_f)/\hbar[(\omega_1-\omega_2-\omega_{fi}) - i\Gamma] + (\chi_{R2}^{(3)})_{NR}. \qquad \text{(S-10)}$$

If the field at ω_1 is not at resonance with some direct transitions

in the medium, then for each photon absorbed at ω_1, there is a photon emitted at ω_2. Applying this conservation law to Eq. (S-8), we readily find

$$I_m\chi_{R1}^{(3)} = - I_m\chi_{R2}^{(3)}$$

and with the help of the Kramers-Kronig relation, we obtain

$$\chi_{R1}^{(3)} = (\chi_{R2}^{(3)})^* \tag{S-11}$$

which is the well-known symmetry relation for Raman susceptibilities [S.31].

With the conservation of number of photons, $[\varepsilon^{1/2}(\omega_1)|\mathcal{E}_1|^2/\omega_1 + \varepsilon^{1/2}(\omega_2)|\mathcal{E}_2|^2/\omega_2] = K$, the solution of Eq. (S-8) is

$$\frac{|\mathcal{E}_1(z)|^2}{|\mathcal{E}_1(z)|^2-\omega_1 K/\varepsilon^{1/2}(\omega_1)} = \frac{|\mathcal{E}_1(0)|^2}{|\mathcal{E}_1(0)|^2-\omega_1 K/\varepsilon^{1/2}(\omega_1)}\, e^{-\omega_1 K G_R z/\varepsilon^{1/2}(\omega_1)|\mathcal{E}_1|^2}$$

$$\frac{|\mathcal{E}_2(z)|^2}{|\mathcal{E}_2(z)|^2-\omega_2 K/\varepsilon^{1/2}(\omega_2)} = \frac{|\mathcal{E}_2(0)|^2}{|\mathcal{E}_2(0)|^2-\omega_2 K/\varepsilon^{1/2}(\omega_2)]}\, e^{+\omega_2 K G_R z/\varepsilon^{1/2}(\omega_2)|\mathcal{E}_1|^2}. \tag{S-12}$$

If $|\mathcal{E}_1|^2 \gg |\mathcal{E}_2|^2$, we have the familiar result

$$|\mathcal{E}_2(z)|^2 = |\mathcal{E}_2(0)|^2 \exp\,(G_R z) \tag{S-13}$$

which shows explicitly the exponential growth of the Stokes field.

In the case where the pump and Stokes waves propagate into the medium with a plane boundary at $z = 0$ along directions other than $\hat{z}$, the wave vectors k_1 and k_2 in Eq. (S-8) should be replaced by the projections of $\vec{k}_1$ and $\vec{k}_2$ along $\hat{z}$. This is obvious since $\mathcal{E}_1$ and $\mathcal{E}_2$ are only functions of z.

S2.2 RAMAN SUSCEPTIBILITIES

The microscopic expression for $\chi_R^{(3)}$ can of course be obtained directly from quantum mechanical perturbation calculation. The derivation is straightforward but tedious [S.22, 31,32]. We can, however, derive it very simply by realizing that so far as the response of the material to the field is concerned, a two-photon process can be considered as an equivalent one-photon process.

Consider the two-photon transition probability given by Eq. (S-1). It can be obtained directly from first-order perturbation if we regard the transition as a direct transition with an effective interaction Hamiltonian

$$\mathcal{H}'_{eff} = - ME_1E_2^* + \text{complex conjugate (c.c.)}. \qquad \text{(S-14)}$$

This can be proved readily if we remember $E = (2\pi\hbar c^2/\omega)^{1/2}a$ and $E^* = (2\pi\hbar c^2/\omega)^{1/2}a^+$, and use the golden rule to derive $dW_{fi}/d(\hbar\omega)$.

Similarly, we can also derive $\chi_R^{(3)}$ by using $\mathcal{H}'_{eff}$ in the equation for linear polarization [S.33]. We then have for the third-order nonlinear polarization $\vec{P}^{(3)}$,

$$\hat{e}_1 \cdot \vec{P}^{(3)}_{(\omega_1)} = \hat{e}_1 \cdot \overleftrightarrow{\chi}^{(3)}_{R1} \cdot \vec{E}_1\vec{E}_2\vec{E}_2^* = - N \frac{|\langle f|ME_2^*|i\rangle|^2(\rho_i-\rho_f)}{\hbar(\omega_1-\omega_2-\omega_{fi}+i\Gamma)} E_1 \qquad \text{(S-15)}$$

where for simplicity, we have neglected the non-resonant term. This equation together with $\chi^{(3)}_{R2} = \chi^{(3)*}_{R1} \equiv \hat{e}_1 \cdot \overleftrightarrow{\chi}^{(3)*}_{R1} : \hat{e}_1\hat{e}_2\hat{e}_2$ leads immediately to the same microscopic equation for χ_{R2} given in Eq. (S-10) with $(\chi^{(3)}_{R2})_{NR}$ neglected.

More generally, Eq.(S-10) can also be derived by considering the states $|i\rangle$ and $|f\rangle$ being coherently admixed by the interaction Hamiltonian $\mathcal{H}'_{eff}$. Let us denote the perturbed states as $|i'\rangle$ and $|f'\rangle$. They should obey the Schrodinger equation

$$\begin{aligned} -i\hbar\partial\langle f'|/\partial t &= \langle f'|(\mathcal{H}_o+\mathcal{H}'_{eff} \\ i\hbar\partial|i'\rangle/\partial t &= (\mathcal{H}_o+\mathcal{H}'_{eff})|i'\rangle \end{aligned} \qquad \text{(S-16)}$$

where $\mathcal{H}_o$ is the unperturbed Hamiltonian for the material system. If we use the interaction representation, we then have in the first-order approximation

$$-\hbar(i\frac{\partial}{\partial t} -\omega_{fi}+i\Gamma)\langle f'|i\rangle = \hbar(i\frac{\partial}{\partial t} -\omega_{fi}+i\Gamma)\langle f|i'\rangle = \langle f|\mathcal{H}'_{eff}|i\rangle. \qquad \text{(S-17)}$$

Here, we have inserted a phenomenological damping constant Γ for ω_{fi}. With $\mathcal{H}'_{eff}$ in Eq. (S-14), the solution of Eq. (S-17) at frequency $\omega_1-\omega_2$ is

$$-\langle f'|i\rangle = \langle f|i'\rangle = - M_{fi}E_1E_2^*/\hbar(\omega_1-\omega_2-\omega_{fi}+i\Gamma). \qquad \text{(S-18)}$$

The nonlinear polarization induced by this perturbation is given by

$$P^{(3)}(\omega_2) = N \langle -\partial \mathcal{H}'_{eff}/\partial E_2^* \rangle$$

$$\cong (\langle f|i'\rangle^* \rho_i + \langle f'|i\rangle^* \rho_f) N M_{fi} E_1$$

$$= \langle f'|i'\rangle^* (\rho_i - \rho_f) N M_{fi} E_1. \qquad \text{(S-19)}$$

Here again, we have considered only the resonant term. Using the expression for $\langle f|i'\rangle$ in Eq. (S-18), we obtain again the same microscopic expression for $\chi^{(3)}_{R2}$.

A matter of interest here is that we can consider $\psi_i = \langle f|i'\rangle$ and $\psi_f = \langle f'|i\rangle$ ($\psi \equiv \psi_i = -\psi_f$) physically as excitational waves (at frequency $\omega_1 - \omega_2$) in the medium [S.16]. They are coupled with E_1 and E_2 via the coupling energy

$$\langle \mathcal{H}'_{eff} \rangle = \langle i'|\mathcal{H}_{eff}|i'\rangle \rho_i + \langle f'|\mathcal{H}_{eff}|f'\rangle \rho_f$$

$$= -M_{fi}(\rho_i - \rho_f) E_1 E_2^* \psi^* + \text{c.c.} \qquad \text{(S-20)}$$

Following Eq. (S-17), these two waves obey the driven wave equations

$$\hbar\left(i\frac{\partial}{\partial t} - \omega_{fi} + i\Gamma\right)\psi_i = +\frac{\partial \langle \mathcal{H}'_{eff} \rangle}{\partial(\rho_i \psi_i^*)} = -M_{fi} E_1 E_2^*$$

$$\hbar\left(i\frac{\partial}{\partial t} - \omega_{fi} + i\Gamma\right)\psi_f = -\frac{\partial \langle \mathcal{H}'_{eff} \rangle}{\partial(\rho_f \psi_f^*)} = -M_{fi} E_1 E_2^*. \qquad \text{(S-21)}$$

Through the coupling with E_1 and E_2, these excitational waves induce the nonlinear polarizations

$$P^{(3)}(\omega_1) = -N\partial\langle\mathcal{H}'_{eff}\rangle/\partial E_1^* = NM_{fi}^* E_2 \psi(\rho_i - \rho_f)$$

$$P^{(3)}(\omega_2) = -N\partial\langle\mathcal{H}'_{eff}\rangle/\partial E_2^* = NM_{fi} E_1 \psi^*(\rho_i - \rho_f) \qquad \text{(S-22)}$$

which then in turn act as the sources in the driven wave equations for E_1 and E_2 in Eq. (S-5). Stimulated Raman scattering (SRS) is now simply the result of nonlinear coupling of the three waves $\psi_i = -\psi_f$, E_1, and E_2, and can be obtained from the solution of the coupled Eqs. (S-5) and (S-21). Note that except the population factors ρ_i and ρ_f which appear to have quantum origins, we can now treat both the material excitation and the radiation as classical waves and SRS as the result of nonlinear coupling of these classical waves.

We have so far assumed ρ_i and ρ_f constant. However, when the field intensities are high so that the Raman transition probability W_{if} is large, the populations ρ_i and ρ_f can be changed appreciably during the Raman process. Directly from physical consideration, we can write the rate equations for ρ_i and ρ_f as [S.32,34]

$$\frac{\partial \rho_i}{\partial t} = -\left(W_{fi}\rho_i - W_{if}\rho_f\right) + \left(\frac{\partial \rho_i}{\partial t}\right)_{\text{damping}}$$

$$\frac{\partial \rho_f}{\partial t} = \left(W_{fi}\rho_i - W_{if}\rho_f\right) + \left(\frac{\partial \rho_f}{\partial t}\right)_{\text{damping}}$$

$$\hbar\omega_{fi}\left(W_{fi}\rho_i - W_{if}\rho_f\right) = \frac{1}{2}\left[\frac{\partial P^{(3)}(\omega_1)^*}{\partial t} E_1 + \frac{\partial P^{(3)}(\omega_2)^*}{\partial t} E_2\right] + \text{c.c.}$$

$$= \frac{1}{2}\, i\omega_{fi} N\left[M_{fi} E_1 E_2^* \psi^* - M_{fi}^* E_1^* E_2 \psi\right](\rho_i - \rho_f). \qquad \text{(S-23)}$$

In the simple case where $(\partial\rho/\partial t)_{\text{damping}}$ is dominated by random relaxation between $|i\rangle$ and $|f\rangle$, we have

$$\Delta\rho = \rho_f - \rho_f^o = -\left(\rho_i - \rho_i^o\right)$$

$$\frac{\partial \Delta\rho}{\partial t} + \frac{\Delta\rho}{T_1} = \left(W_{fi}\rho_i - W_{if}\rho_f\right) \qquad \text{(S-24)}$$

where ρ_i^o and ρ_f^o are the populations at thermal equilibrium, and T_1 is the well-known longitudinal relaxation time as distinguished from the transverse relaxation time $T_2 \equiv 1/\Gamma$. Raman transitions and Raman susceptibilities in this saturation limit are the subject of discussion in Ref. [S.32].

The above discussion deals with localized electronic excitations but the general formalism is of course valid for any material excitation, e.g., molecular vibration, phonon, [S.22] magnon [S.35], exciton, plasmon [S.36], polariton [S.37], etc. The wave equations are generally different for different types of excitations; Eq. (S-21) should therefore be replaced by wave equations appropriate for the excitation involved in

the problem. The coupling constant M_{fi} in Eqs. (S-21) and (S-22) should also be changed accordingly. There is also the difference between boson-type excitations and localized excitations between two levels. For localized excitations, we use Eq. (S-24), but for boson-type excitations, we have $W_{fi}\rho_i \propto 1+n_\psi$, $W_{if}\rho_f \propto n_\psi$, and $(\frac{\partial}{\partial t} + \frac{1}{T_1})(n_\psi - \bar{n}_\psi) = W_{fi}\rho_i - W_{if}\rho_f$, where n_ψ is the average number of bosons at thermal equilibrium. The general formalism is also valid for any two-photon transition process. For example, it can be applied to the problem of two-photon absorption and second-harmonic generation near an excitonic resonance, e.g., in CuCl [S.38-40].

S.2.3 PARAMETRIC COUPLING BETWEEN PHOTONS AND PHONONS

In this section, we consider the special case where molecular vibrations or phonons in the medium are being excited in the Raman process. This is the most important case since at least 90% of the published Raman work deals with Raman scattering by molecular vibrations or phonons. We can of course use quantum mechanics to describe molecular vibration or phonons [S.3,25]. However, as shown in the previous section, we can describe stimulated Raman amplification classically as the result of parametric coupling between electromagnetic waves and material excitational waves. We shall present only the classical description here [S.22].

Let us consider first the coupling between photon and phonon waves. It is governed by the interaction energy of Eq. (S-20) with ψ replaced by $(2\omega_3/\hbar)^{1/2}Q$ where Q is the phonon wave at frequency $\omega_3 \equiv \omega_1-\omega_2$. Comparing with the usual expression of $\langle\mathcal{H}'_{eff}\rangle = -(\partial\alpha/\partial Q)E_1E_2^*Q^* + c.c.$, we have $M_{fi} = (\partial\alpha/\partial Q)/(2\omega_3/\hbar)^{1/2}$ where α is the polarizability [S.22]. The coupling constant M_{fi} can also be obtained from the general expression of M in Eq. (S-1). As shown in Eqs. (S-9) and (S-10), the spontaneous

Raman scattering cross-section $d\sigma/d\Omega$ is directly proportional to $|M_{fi}|^2$. We shall not go further into the detailed microscopic theory of $d\sigma/d\Omega$ for this case since it has already been dealt with in the other chapters of this book. For our purposes, we only need to remember that the coupling constant M_{fi} can be easily deduced from the spontaneous Raman cross-sections $d\sigma/d\Omega$.

The wave equation for phonons is given by [S.22]

$$[\beta\nabla^2 + \frac{\partial^2}{\partial t^2} + 2\Gamma \frac{\partial}{\partial t} + \omega_o^2]Q = -\partial\langle\mathcal{H}'_{eff}\rangle/\partial Q^*(\rho_i - \rho_f)$$

$$= (\frac{2\omega_3}{\hbar})^{1/2} M_{fi} E_1 E_2^* \qquad \text{(S-25)}$$

where β is a constant which characterizes the phonon dispersion near $k = 0$, ω_o is the phonon frequency at $k = 0$, and Γ is again the damping constant. SRS by phonons is then fully described by the solution of the three coupled wave equations (S-25), and (S-5), where $P^{(3)}(\omega_1)$ and $P^{(3)}(\omega_2)$ are given by Eq. (S-22) with $\psi_i = -\psi_f$ replaced by $(2\omega_3/\hbar)^{1/2}Q$.

Several different cases arise depending on the values of β and ω_o. If $\beta < 0$, and $\omega_o = 0$, then Eq. (S-25) is the equation for an acoustic wave. Stimulated light scattering by acoustic phonons is known as stimulated Brillouin scattering [S.41]. From the above discussion we see clearly that stimulated Brillouin scattering is simply a special class of SRS. We shall not discuss stimulated Brillouin scattering any further in this review article. For optical phonon waves, we have $\omega_o \neq 0$ and $\beta \neq 0$ (usually $\beta > 0$). In the limit where interaction between molecules is negligible, the optical phonons become dispersionless and reduce essentially to molecular vibrations. It is SRS by optical phonons or molecular vibrations which one normally encounters in the studies of SRS.

The wave vector of photons and phonons involved in SRS is of the order of 10^5 cm^{-1} or less. Hence, the $\beta\nabla^2 Q$ term in Eq. (S-25) for optical phonons is often negligible. We then have

$$Q = -(2\omega_3/\hbar)^{1/2} M_{fi} E_1 E_2^* / [\omega_3^2 - \omega_{fi}^2 + 2\omega_3 \Gamma] \qquad \text{(S-26)}$$

where $\omega_3 = \omega_1 - \omega_2$. From Eq. (S-22) with the non-resonant term included, we find for $\omega_3 \sim \omega_o$,

$$\chi_{R2}^{(3)} = - N|M_{fi}|^2 (\rho_i - \rho_f)/\hbar(\omega_3 - \omega_{fi} - i\Gamma) + (\chi_{R2}^{(3)})_{NR} \qquad \text{(S-27)}$$

which is identical to Eq. (S-10). Consequently, the expression for the Raman gain G_R in Eq. (S-9) and the solution of the coupled wave equations in Eq. (S-12) (assuming ρ_i and ρ_f constant) are still valid for the present case.

S.2.4 STOKES - ANTISTOKES COUPLING

We have assumed so far that in SRS only electromagnetic waves at ω_1 and ω_2 are present in the medium. We shall now see that in general Stokes and antiStokes waves ($\omega_1 \pm \omega_3$) are in fact simultaneously generated in the stimulated Raman process, even at 0°K. This is very different from the spontaneous scattering case where no antiStokes scattering occurs at 0°K.

We can see most clearly the simultaneous Stokes - antiStokes generation from the coupled wave approach. The incoming wave at ω_1 first beats with the waves at $\omega_1 \pm \omega_3$ to drive the material excitational wave at

ω_3. The material excitation in turn beats with the incoming wave at ω_1 to create nonlinear polarizations at $\omega_1 \pm \omega_3$ [S.26,27]. These nonlinear polarizations then act as the sources to amplify Stokes ($\omega_1 - \omega_3$) and antiStokes ($\omega_1 + \omega_3$) waves in the medium.

Let us use subindices s and a to denote Stokes and antiStokes respectively. Then, we have $\omega_1 - \omega_s = \omega_a - \omega_1 = \omega_3$. The interaction energy for coupling between E_1, E_s, E_a, and ψ is

$$\langle \mathcal{H}'_{eff} \rangle = - M^s_{fi}(\rho_i - \rho_f) E_1 E_s^* \psi^* - M^a_{fi}(\rho_i - \rho_f) E_a E_1^* \psi^* + c.c. \qquad (S\text{-}28)$$

where M^s_{fi} and M^a_{fi} are identical to M_{fi}, except that ω_s replaces ω_2 in M^s_{fi} and ω_a and ω_1 replace ω_1 and ω_2 respectively in M^a_{fi}. If dispersion in M_{fi} is negligible, then $M^s_{fi} \cong M^a_{fi}$. The nonlinear polarizations at ω_s, ω_a, and ω_1 are now given by

$$\begin{aligned}
\hat{e}_s \cdot \vec{P}^{(3)}(\omega_a) &= -N\partial\langle \mathcal{H}'_{eff} \rangle / \partial E_s^* = N M^s_{fi}(\rho_i - \rho_f) E_1 \psi^* \\
\hat{e}_a \cdot \vec{P}^{(3)}(\omega_a) &= -N\partial\langle \mathcal{H}'_{eff} \rangle / \partial E_a^* = N (M^a_{fi})^* (\rho_i - \rho_f) E_1 \psi \\
\hat{e}_1 \cdot \vec{P}^{(3)}(\omega_1) &= -N\partial\langle \mathcal{H}'_{eff} \rangle / \partial E_1^* = [(M^s_{fi})^* E_s \psi + M^a_{fi} E_a \psi^*](\rho_i - \rho_f)
\end{aligned} \qquad (S\text{-}29)$$

where we have not included the nonresonant terms. The driven wave equation for ψ is

$$\hbar\left(i\frac{\partial}{\partial t} - \omega_{fi} + i\Gamma\right)\psi = -M_{fi}^{s}E_1E_s^* - M_{fi}^{a}E_aE_1^*. \qquad \text{(S-30)}$$

Stokes and antiStokes generation in SRS is now governed by the solution of the four coupled wave equations, i.e., Eq. (S-30) and the wave equations for E_1, E_s, and E_a.

We can first obtain ψ from Eq. (S-30):

$$\psi = -[M_{fi}^{s}E_1E_s^* + M_{fi}^{a}E_aE_1^*]/\hbar(\omega_3-\omega_{fi} + i\Gamma). \qquad \text{(S-31)}$$

Then, with the above expression for ψ inserted in Eq. (S-29), the wave equations for E_1, E_s, E_a in the steady state becomes [S.22]

$$\hat{e}_1 \cdot [\nabla\times(\nabla\times\vec{E}_1) - \frac{\omega_1^2}{c^2}\overleftrightarrow{\varepsilon}_1 \cdot \vec{E}_1] = \frac{4\pi\omega_1^2}{c^2}[\chi_{ss}^{(3)}|E_s|^2E_1 + (\chi_{sa}^{(3)} + \chi_{sa}^{(3)*})E_sE_aE_1^* + \chi_{aa}^{(3)}|E_a|^2E_1]$$

$$\hat{e}_s \cdot [\nabla\times(\nabla\times\vec{E}_s) - \frac{\omega_s^2}{c^2}\overleftrightarrow{\varepsilon}_s \cdot \vec{E}_s] = \frac{4\pi\omega_s^2}{c^2}[\chi_{ss}^{(3)}|E_1|^2E_s + \chi_{sa}^{(3)}E_1^2E_a^*]$$

$$\hat{e}_a \cdot [\nabla\times(\nabla\times\vec{E}_a) - \frac{\omega_a^2}{c^2}\overleftrightarrow{\varepsilon}_a \cdot \vec{E}_a] = \frac{4\pi\omega_a^2}{c^2}[\chi_{sa}^{(3)*}E_1^2E_s^* + \chi_{aa}^{(3)}|E_1|^2E_a] \qquad \text{(S-32)}$$

where

$$\chi_{ss}^{(3)} = (\chi_s^{(3)})_{NR} - N|M_{fi}^s|^2(\rho_i-\rho_f)/\hbar(\omega_3-\omega_{fi}-i\Gamma)$$

$$\chi_{ss}^{(3)} = (\chi_{sa}^{(3)})_{NR} - NM_{fi}^s M_{fi}^{a*}(\rho_i-\rho_f)/\hbar(\omega_3-\omega_{fi}-i\Gamma)$$

$$\chi_{aa}^{(3)} = (\chi_{aa}^{(3)})_{NR} - N|M_{fi}^a|^2(\rho_i-\rho_f)/\hbar(\omega_3-\omega_{fi}-i\Gamma). \qquad \text{(S-33)}$$

The solution of Eq. (S-32) is greatly simplified if we can neglect the depletion of the incoming wave E_1 in the SRS process, since then we have just a set of two linearly coupled equations for E_s and E_a. Assuming an isotropic medium with a plane boundary at $z = 0$ and slowly varying amplitudes for E_s and E_a, we readily find [S.22] (see Fig. S.2)

$$E_s = [\mathcal{E}_{s+}\exp(i\Delta K_+ z) + \mathcal{E}_{s-}\exp(i\Delta K_- z)]\exp(i\vec{k}_s\cdot\vec{r} - \alpha_{sz}z)$$

$$E_a^* = [\mathcal{E}_{a+}^*\exp(i\Delta K_+ z) + \mathcal{E}_{a-}^*\exp(i\Delta K_- z)]\exp(-i\vec{k}_a\cdot\vec{r} - (i\Delta k+\alpha_{az})z] \qquad \text{(S-34)}$$

where $$k^2 = \omega^2\varepsilon'/c^2$$

$$\Delta k = 2k_{1z} - k_{sz} - k_{az}, \qquad k_z \equiv \vec{k}\cdot\hat{z}$$

$$\Delta K\pm = \Delta k/2 \pm \{(\Delta k/2)^2 - (\Delta k)\lambda\}^{1/2}$$

$$\lambda = [2\pi\omega_s^2/c^2k_{sz}]\,\chi_{ss}^{(3)}|E_1|^2, \qquad \alpha_z = \omega^2\varepsilon''/c^2k_z = \alpha(k/k_z).$$

For simplicity, we have neglected here the dispersions of the absorption

coefficients α_z and $[2\pi\omega^2/c^2 \mathrm{Re}(\vec{k} \cdot \hat{z})]\chi^{(3)}$. The more general solution with the dispersion included can of course also be written down quite straightforwardly. If $\mathcal{E}_{so}$ and $\mathcal{E}_{ao}$ are the boundary values of $\mathcal{E}_a$ at $z = 0$, then we have

$$\mathcal{E}_{a\pm}/\mathcal{E}_{s\pm} = (\Delta K_{\pm} - \lambda)/\lambda$$

$$\mathcal{E}_{s\pm} = [(-\Delta K_{\mp} + \lambda)\ \mathcal{E}_{so} + \lambda\ \mathcal{E}^*_{ao}]/(\Delta K_{\pm} - \Delta K_{\mp}). \qquad \text{(S-35)}$$

A number of physical results follow immediately from the solution in Eqs.(S-34) and (S-35). a) If the phase mismatch Δk is sufficiently large or $\chi^{(3)}_{ss}|E_1|^2$ sufficiently small so that $|\Delta k| \gg |\lambda|$, then the Stokes and antiStokes fields are effectively decoupled. The two parts of the solution reduce to

$$\begin{cases} \Delta K_- = \lambda \\ |\mathcal{E}^*_a/\mathcal{E}_s| = |\lambda/\Delta k| \ll | \end{cases} \quad \text{and} \quad \begin{cases} \Delta K_+ = -\lambda + \Delta k \\ |\mathcal{E}^*_a/\mathcal{E}_s| = |\Delta k/\lambda| \gg |. \end{cases}$$

(Note that $-\mathrm{Im}(\lambda) = G_R/2$). The first part corresponds to an almost pure Stokes wave with an exponential gain G_R and the second part corresponds to an almost pure antiStokes wave with a gain $-G_R$. These results are what we should expect when there is little Stokes-antiStokes coupling as discussed in previous sections. We notice that at thermal equilibrium, the almost pure antiStokes wave has a negative gain since its energy is now used in SRS to amplify the pump wave. b) If the

linear phase matching condition $\Delta k = 0$ is satisfied, we find $\Delta K_{\pm} = 0$ and $|\mathcal{E}^*_{a\pm}/\mathcal{E}_s| = 1$. There is no exponential gain for both Stokes and antiStokes fields. Although the Stokes-antiStokes coupling is maximum in this case, the positive work done on the Stokes field is exactly compensated by the negative work done on the antiStokes field. This is well known in parametric amplifier theory where no gain can be obtained at $\omega_s = \omega_1 - \omega_3$ if the other side band at $\omega_a = \omega_1 + \omega_3$ is not suppressed.

c) As Δk gradually deviates from zero, the positive exponential gain increases rapidly towards the value G_R as shown in Fig. S.3, while the corresponding $|\mathcal{E}^*_a/\mathcal{E}_s|$ decreases from 1 towards 0. Consequently, at some value of $|\Delta k|$, the antiStokes power generated in this SRS process goes through a maximum. This is shown in Fig. S.4 for two different values of $G_R z$. We therefore expect that the antiStokes radiation appears in the form of double cones in the k-space. For more details on the calculation, the readers should consult Ref. [S.22]. We shall discuss the experimental results in terms of these theoretical predictions in a later section.

S.2.5 HIGHER-ORDER RAMAN EFFECTS

Intense higher-order Stokes and antiStokes fields can also be generated in SRS [S.5-10]. They are generated by the successively induced third-order nonlinear polarizations $P^{(3)}$ at appropriate frequencies. For example, the second Stokes field E_{s2} can be generated by

$$P^{(3)}(\omega_{s2}) = \chi^{(3)}_{s\alpha} E_s^2 E_1^* + \chi^{(3)}_{s\beta} E_1 E_s E_a^*.$$

They should appear most strongly around the phase-matching directions

given by $\vec{k}_{s2} = \vec{k}_s + \vec{k}_s' - \vec{k}_1$ and $\vec{k}_{s2} = \vec{k}_1 + \vec{k}_s - \vec{k}_a$. The generation of second Stokes is clearly a higher-order effect since $P^{(3)}(\omega_{s2})$ here is linearly proportional to the pump field $|E_1|$ while $P^{(3)}(\omega_s)$ and $P^{(3)}(\omega_a)$ are proportional to $|E_1|^2$. When the first Stokes $E(\omega_s)$ becomes intense enough, E_{s2} can also be generated through $P^{(3)}(\omega_{s2}) = \chi^{(3)}_{s\gamma}|E_s|^2E_{s2} + \chi^{(3)}_{s\delta}E_s^2E^*_{a2}$, where E_{a2} is the second antiStokes. Similarly, the nonlinear polarizations responsible for the generation of other higher-order Stokes and antiStokes fields can be written down easily. The complete description of these higher-order stimulated Raman effects should then be obtained from the solution of the many wave equations which are nonlinearly coupled through the nonlinear polarizations. This is of course a formidable task in general.

In the special case where we can assume that only Stokes waves along $+\hat{z}$ are generated, the set of coupled wave equations is [S.22]

$$[\partial^2/\partial z^2 + (\omega_1\varepsilon_1/c^2)]E_1 = -(4\pi\omega_1^2/c^2)\chi^{(3)*}_{s1}|E_s|^2E_1$$

$$[\partial^2/\partial z^2 + (\omega_s\varepsilon_s/c^2)]E_s = -(4\pi\omega_s^2/c^2)[\chi^{(3)}_{s1}|E_1|^2E_s+\chi^{(3)*}_{s2}|E_{s2}|^2E_s]$$

$$[\partial^2/\partial z^2 + (\omega_{s2}\varepsilon_{s2}/c^2)]E_{s2} = -(4\pi\omega_{s2}^2/c^2)[\chi^{(3)}_{s2}|E_{s2}|^2E_s+\chi^{(3)*}_{s3}|E_{s3}|^2E_{s2}]. \quad \text{(S-36)}$$

The solution of Eq. (S-36) obtained from numerical calculation for infinite plane waves is shown in Fig. S.5 . It is seen that the first Stokes power first increases gradually and then suddenly builds up to a maximum value while the pump power gets almost completely depleted. As z increases further, the first Stokes power remains nearly constant for

a while, and then again suddenly gets depleted into the second Stokes, and so on. This was actually demonstrated in a properly designed experiment by Von der Linde et al [S.42], as we shall see later.

S.3 EXPERIMENTAL OBSERVATIONS

After the accidental discovery of SRS in nitrobenzene [S.4] in 1962, the subject of SRS soon attracted much attention. The earlier detailed experimental studies of SRS were mostly on liquids with large Kerr constants. A typical setup is shown in Fig. S.6. It was then realized that the observed Raman output was much too intense to be accounted by the theory. For example, from the spontaneous Raman data, one can calculate, by using Eq. (S-3), the maximum Raman gain for nitrobenzene to be 2.8×10^{-3} cm/MW (see Table S.1), i.e., in order to amplify the Raman radiation from the noise level by e^{28} times in a 10-cm cell, one would need an input laser intensity of 1000 MW/cm^2. The Q-switched laser pulse intensity used in the experiments was, however, always around 100 MW/cm^2 or less, which should not be sufficient to generate any detectable Raman radiation. This observed gain anomaly [S.43] together with many other related anomalous effects such as forward-backward asymmetry [S.44], spectral broadening [S.44], anomalous antiStokes rings [S.44,45], etc., had stimulated a lot of research acitivites on the subject. Only several years later, people began to understand thatmost of these anomalous effects were actually induced by self-focusing of the input beam [S.46]. Therefore, before we compare the experimental results with the theory, we should discuss briefly how self-focusing affects SRS.

S.3.1 ANOMALOUS EFFECTS DUE TO SELF-FOCUSING

The gain anomaly is illustrated in Fig. S.7. The curve of first Stokes intensity versus input power shows a sharp threshold. The slope

at the threshold yields an anomalously large Raman gain which cannot be understood from the theory of SRS. Now, this is known to be due to self-focusing. Self-focusing arises because of the existence of a positive field-induced refractive index in the medium. Consider a beam with finite cross-section. The central portion, which is more intense, sees a larger refractive index and therefore propagates more slowly than the edge. Consequently, the wavefront is distorted. Since the rays should always propagate perpendicular to the wavefront, they then appear to bend towards the axis and self-focus to a point. The focus is at the position [S.47]

$$z_f(t) \cong K/[\sqrt{P(t)} - \sqrt{P_{cr}}]$$

where K and P_{cr} are constants depending on the beam characteristics and material properties. As the laser power P increases, z_f decreases. When z_f first appears in the medium, the intense focus generates the Raman radiation readily. This then explains the observed sharp Raman threshold. It has now been clearly established that SRS in self-focusing liquids is in fact always initiated from the focal region [S.48,49].

Self-focusing also explains the forward-backward asymmetry in SRS. For an input beam with a finite cross-section, the Raman intensities in different directions are expected to be different because of the different active lengths, but the forward and the backward Raman intensities are supposed to be equal by symmetry. The experimental results in self-focusing liquids, however, show a clear forward-backward asymmetry, as seen in Fig. S.7. This is again due to self-focusing. Since SRS is

first initiated from the first focus at or near the end of the cell, the forward and backward Raman radiation should experience very different Raman amplification. Moreover, the fact that the backward Raman radiation always meets head-on with the undepleted incoming laser beam could lead to a very short sub-nanosecond Raman pulse [S.50].

Self-focusing also imposes a strong frequency modulation on the beam. This then explains the observed spectral broadening of both laser and Raman radiation in self-focusing liquids [S.51]. In non-self-focusing media, the spectral broadening may be due to successive beats of laser and Raman radiation to many orders [S.52,53].

First-order antiStokes radiation should appear around the directions defined by $\vec{k}_a = 2\vec{k}_1 - \vec{k}_s$. However, in self-focusing liquids, another cone of antiStokes radiation at somewhat larger angle from the axis can often be observed [S.45]. This is presumably due to antiStokes emitted in the filamentary focal region, because the condition of phase matching along the surface of the filament is now important [S.54].

S.3.2 RAMAN OSCILLATION IN NON-SELF-FOCUSING MEDIA

Even in non-self-focusing media, study of SRS using the setup in Fig. S.6 shows a sharp threshold in the growth of Stokes intensity versus input laser power. An example is shown in Fig. S.8, which gives the Stokes output versus the laser input in liquid nitrogen [S.55]. Self-focusing was not observed in this case. As the laser power increases, the Stokes output first increases linearly as a result of spontaneous scattering and then grows quasi-exponentially. At a certain input power I_{Li}, the Stokes output shows a sudden rise. Finally, it levels off because of depletion of laser power.

This sharp threshold was first believed to be due to feedback from Rayleigh scattering [S.55]. Very recently, Sparks [S.25] has pointed out that this is in fact an intrinsic behavior of Raman oscillation resulting from parametric instability. Using the full quantum description (Eq. (S-3a) with $W_{fi}\rho_i \propto n_1(n_2+1)(n_2+1)$, $W_{if}\rho_f \propto (n_1+1)n_2n_2$, and $(\frac{\partial}{\partial t} + \frac{1}{T_1})(n_2 - \bar{n}_a) = W_{fi}\rho_i - W_{if}\rho_f$, where $\bar{n}_2$ is the number of thermally excited phonons), he finds a solution of the coupled equations. His calculated results for SRS in liquid N_2 agree very well with experimental data, as shown in Fig. S.8. However, it should be pointed out that for liquid N_2, it is probably more appropriate to use the localized molecular vibration model rather than the phonon model, i.e., we should use ρ_i, ρ_f, and Eq. (S-24) instead of n_2 and the differential equation for n_2.

S.3.3 RAMAN GAIN MEASUREMENTS

The setup in Fig. S.6 is of course only good for studying Raman oscillation. In order to study stimulated Raman amplification, one must not use a single oscillator system, but should use a combined oscillator-amplifier system [S.57]. A typical setup is shown in Fig. S.9. The Raman gain can be obtained by measuring the ratio of the Stokes input to the Stokes output of the amplifier. In Fig. S.10, the results of Lallemand et al. [S.57] on hydrogen gas are shown to be in good agreement with the theoretical curve. Such a Raman gain measurement is, however, not very successful in self-focusing liquids because self-focusing would occur in the amplifier before the amplification factor differs appreciably from 1. [S.58].

S.3.4 ANTISTOKES AND HIGHER-ORDER RAMAN RADIATION

Stimulated antiStokes radiation was first observed by Terhune [S.10]. As shown in Fig. S.11, it appears in the form of bright multi-colored rings. Different rings often correspond to different orders of antiStokes. In liquids, antiStokes rings up to the 4th order can be easily photographed on color film. Chiao and Stoicheff [S.12] showed in calcite that the antiStokes is actually emitted with cone angles given by the phase-matching relation $\vec{k}_{a,n} = \vec{k}_{a,n-1} + \vec{k}_1 - \vec{k}_{s,n}$, where the integer n indicates the order. We may recall that the theory (Section S.2.4) predicts for the first antiStokes a ring with a central dark band at the phase-matching directions. The reason the dark band was not observed is presumably due to the fact that a practical laser beam has a spread in the $\vec{k}$-space which tends to smear the dark band in the antiStokes ring.

Garmire made a detailed study on the antiStokes rings produced in self-focusing liquids [S.45]. Two sets of cones were observed, Class I and Class II. Class I appeared at the normal phase-matching directions and Class II at some anomalous directions presumably determined by surface phase matching along the filaments created by self-focusing [S.45,54].

Higher-order Stokes radiation has also been observed mostly along the axis in the forward and backward directions. Quantitative studies of generation of higher-order Stokes radiation are generally difficult because of the many competing nonlinear processes present. Von der Linde et al. [S.42] using subnanosecond laser pulses were, however, able to carry out a quantitative study in a special case. The short input pulse effectively suppresses both the stimulated Brillouin scattering and the

backward Raman radiation. The effect of self-focusing can also be minimized by using high pulse intensity. Then, the forward SRS becomes the only effective nonlinear process in the medium. This is just the condition under which Eq. (S-36) is valid. Figure S.12 shows that the experimental results agree very well with the theoretical curves calculated from Eq. (S-36), taking into account the real beam profile.

S.3.5 STIMULATED ANTISTOKES ABSORPTION

As seen in Section S.2.4, the gain of the stimulated first-order antiStokes radiation is negative in directions where the Stokes-antiStokes coupling is weak. With both laser and antiStokes radiation present, the laser field will be amplified at the expense of the antiStokes. Thus, if the laser beam and a beam from a broadband source around ω_a propagates together in the medium, we expect to find a dark absorption band at ω_a in the broadband output spectrum. This was observed by Jones and Stoicheff [S.59], and has been suggested as a useful spectroscopic technique to study molecular vibration.

S.3.6 COMPETITION BETWEEN DIFFERENT RAMAN MODES

Under normal conditions with nanosecond pulse excitation, only one Raman mode which has the maximum Raman gain participates in SRS. This is usually the Raman mode with both large cross-section and narrow linewidth. The effective depletion of laser power into this Raman mode forbids SRS to occur with other Raman modes. In transient SRS, it is, however, possible to have several Raman modes show up simultaneously, as we shall see later.

S.3.7 COMPETITION BETWEEN STIMULATED RAMAN SCATTERING AND OTHER NON-LINEAR OPTICAL PROCESSES

We have already seen the effect of self-focusing on SRS. Other nonlinear processes, such as stimulated Brillouin scattering, two-photon absorption, etc., may also affect SRS. They may compete with SRS in depleting the laser power and consequently suppress SRS [S.50]. Quantitative studies of the influence of other nonlinear processes on SRS have not yet been done.

S.3.8 STIMULATED RAMAN SCATTERING IN SOLIDS

We give in Table S.2 a list of crystals in which SRS has been observed. The study of SRS in crystals has not been as extensive as in liquids mainly because a crystal is less flexible for investigation than a liquid and often much more expensive.

S.4 STIMULATED POLARITON SCATTERING

In more general cases, the material excitation ψ discussed in Section S.2 can be excited not only by Raman process (or two-photon), but also by direct infrared (one-photon) absorption. In other words, the excitation is both infrared and Raman active. This happens for example with phonons in polar crystals. Coupling of lattice vibration and infrared wave was first studied by Huang [S.60]. In general, the mixed excitational wave resulting from direct coupling of photon and material excitation is known as polariton [S.6], and obeys the so-called polariton dispersion curve.

SRS in such a medium will excite the mixed infrared and material excitational wave or simply the polariton wave, and therefore is called stimulated polariton scattering (SPS). The theory of SPS has been discussed by Loudon [S.37], by Butcher et al. [S.37], by Shen [S.62], by Henry and Garrett [S.63], and by many others [S.64]. We shall present the coupled-wave approach here [S.16,62].

Consider four waves interacting with one another in SPS: the laser E_1, the Stokes E_s, the infrared E_3, and the material excitation ψ. If we assume negligible depletion of the laser power, then the wave equations for the other three waves can be written as (see Section S.2)

$$[\nabla^2 + (\omega_s^2\varepsilon_s/c^2)]E_s = -(4\pi\omega_s^2/c^2)P^{NL}(\omega_s)$$

$$[\nabla^2 + (\omega_3^2\varepsilon_3/c^2)]E_3 = -(4\pi\omega_3^2/c^2)[P^{(1)}(\omega_3) + P^{NL}(\omega_3)]$$

$$\hbar(\omega_3 - \omega_{fi} + i\Gamma)\psi = F^{(1)} + F^{NL} \qquad \text{(S-37)}$$

where $\omega_3 = \omega_1 - \omega_s$.

We have assumed ψ has negligible dispersion and has a resonant frequency ω_{fi}. The direct coupling between E_3 and ψ leads to an effective interaction energy

$$\langle\mathcal{H}^{(1)}_{eff}\rangle = -NA_{fi}(\rho_i - \rho_f)\,\psi^* E_3 + c.c. \qquad \text{(S-38)}$$

where $A_{fi}E_3 = \langle f|\mathcal{H}'|i\rangle$ and $\mathcal{H}'$ is the usual interaction Hamiltonian between light and matter. We then obtain

$$P^{(1)}(\omega_3) = -\partial\langle\mathcal{H}^{(1)}_{eff}\rangle/\partial E^*_3 = NA^*_{fi}\ (\rho_i - \rho_f)\psi$$

$$F^{(1)} = +\partial\langle\mathcal{H}^{(1)}_{eff}\rangle/\partial[\psi^* N(\rho_i - \rho_f)] = -A_{fi}E_3. \qquad \text{(S-39)}$$

The nonlinear coupling between waves leads to

$$\langle\mathcal{H}^{NL}_{eff}\rangle = -NM^s_{fi}(\rho_i - \rho_f)E_1E^*_s\psi^* - \chi^{(2)}E_1E^*_sE^*_3 + c.c. \qquad \text{(S-40)}$$

from which we find

$$P^{NL}(\omega_s) = \chi^{(2)}E_1E^*_3 + NM^s_{fi}(\rho_i - \rho_f)E_1\psi^*$$

$$P^{NL}(\omega_3) = \chi^{(2)}E_1E^*_s$$

$$F^{NL} = -M^s_{fi}E_1E^*_s. \qquad \text{(S-41)}$$

Elimination of ψ in Eq. (S-37) yields [S.16]

$$[\nabla^2 + (\omega_s^2/c^2)(\varepsilon^*_s)_{eff}]E^*_s = -(4\pi\omega_s^2/c^2)\ \chi^{(2)}_{eff}E_1E_3$$

$$[\nabla^2 + (\omega_3^2/c^2)(\varepsilon_3)_{eff}]E_3 = -(4\pi\omega_3^2/c^2)\ \chi^{(2)}_{eff}E_1E^*_s \qquad \text{(S-42)}$$

where

$$(\varepsilon_s^*)_{eff} = \varepsilon_s^* + 4\pi\, \chi_R^{(3)} |E_1|^2$$

$$\chi_R^{(3)} = - N|M_{fi}^s|^2 (\rho_i - \rho_f)/\hbar(\omega_3 - \omega_{fi} + i\Gamma)$$

$$(\varepsilon_3)_{eff} = \varepsilon_3 - N|A_{fi}|^2 (\rho_i - \rho_f)/\hbar(\omega_3 - \omega_{fi} + i\Gamma)$$

$$\chi_{eff}^{(2)} = \chi^{(2)} - N\, A_{fi}^* M_{fi}^s (\rho_i - \rho_f)/\hbar(\omega_3 - \omega_{fi} + i\Gamma).$$

(S-43)

We have assumed for simplicity that $A_{fi}^* M_{fi}^s$ is real. Note that $k_3 = (\omega_3/c)(\varepsilon_3)_{eff}^{1/2}$ gives the polariton dispersion curve.

The equations in (S-42) are in the same form as the wave equations governing parametric amplification [S.65]. They are also similar to Eq. (S-32) for Stokes-antiStokes coupling. The solution of Eq. (S-42) is also similar to Eqs. (S-34,35) and can be written down easily. For waves propagating into a medium with a plane boundary at z = 0, we have [S.16]

$$E_s^* = [\mathcal{E}_{s+}^* \exp(i\Delta K_+ z) + \mathcal{E}_{s-}^* \exp(i\Delta K_- z)] \exp(-i\vec{k}_s \cdot \vec{\gamma})$$

$$E_3 = [\mathcal{E}_{3+} \exp(i\Delta K_+ z) + \mathcal{E}_{3-} \exp(i\Delta K_- z)] \exp(i\vec{k}_3 \cdot \vec{r} + i\Delta kz) \quad \text{(S-44)}$$

where

$$k = (\omega/C)(\varepsilon'_{eff})^{1/2}$$

$$\Delta k = k_{1z} - k_{sz} - k_{3z}, \qquad k_z = \vec{k} \cdot \hat{z}$$

$$\Delta K_\pm = \frac{1}{2}(\gamma_s - \gamma_3) \pm \frac{1}{2}[(\gamma_s + \gamma_3)^2 - 4\Lambda]^{1/2}$$

$$\gamma_s = (k_s/2k_{sz})(i\alpha_s + 2k_R)$$

$$k_R = (\omega_s^2/2k_{sz}c^2)4\pi\chi_R|E_1|^2$$

$$\gamma_3 = -\Delta k - i(k_3/2k_{3z})\alpha_3$$

$$\Lambda = (4\pi^2\omega_s^2\omega_3^2/c^2k_{sz}k_{3z})(\chi_{eff}^{(2)})^2|E_1|^2$$

$$|\mathcal{E}_3/\mathcal{E}_s^*| = (\omega_3^2 k_{sz}/\omega_s^2 k_{3z})^{1/2}|\Lambda^{1/2}(\Delta K_\pm + \gamma_3)|. \quad \text{(S-45)}$$

The gain corresponds to $G = -2\ \mathrm{Im}(\Delta K_\pm)$. We consider only the mode with $G > 0$.

Two special cases should be mentioned here. First, if there is neither linear nor nonlinear coupling between E_3 and the other waves, i.e., $A_{fi} = 0$ and $\chi^{(2)} = 0$, then the problem reduces to Stokes generation with $G = G_R$. Second, if the nonlinear coupling between ψ and E_s vanishes, i.e., $M_{fi} = 0$, then the problem reduces to the simple case of parametric amplification [S.65]. The expressions of G and $|\mathscr{E}_3/\mathscr{E}_s^*|$ given here also reduce to those of Henry and Garrett [S.63] when ψ is replaced by $(2\omega_3/\hbar)^{1/2}Q$, the absorption coefficient α_s is neglected, and ε_3 is assumed to be real.

For given ω_3, the gain is a maximum at phase matching $\Delta k = 0$ if the resonance at ω_{fi} is sufficiently narrow. Henry and Garrett [S.63] have calculated G_{max} and the corresponding $|\mathscr{E}_3/\mathscr{E}_s^*|$ for GaP at frequencies around the 366 - cm^{-1} phonon mode. Their results are shown in Fig. S.13. In this case, only a small section below $\omega_{fi} \equiv \omega_o$ can be phase matched. The two terms in $\chi^{(2)}_{eff}$ of Eq. (S-43) are of opposite signs for $\omega_3 < \omega_o$ in GaP. As a result, G_{max} gradually reduces to zero as $\omega_3 \to 250$ cm^{-1}. Sussman [S.66] has made similar calculations for the 248 - cm^{-1} phonon mode of $LiNbO_3$. The results are shown in Fig. S.14. The two terms in $\chi^{(2)}_{eff}$ are now of the same sign for $\omega_3 < \omega_o$ and hence G_{max} increases gradually for $\omega_3 < \omega_o$.

Experimentally, SPS was first observed in $LiNbO_3$ by Kurtz et al. [S.13]. Gelbwachs et al. [S.14] demonstrated the fact that the Stokes frequency can be tuned over a narrow range by adjusting the relative angle between $\vec{k}_1$ and $\vec{k}_s$ to achieve phase matching with ω_3 sitting on the polariton dispersion curve. In a resonator, up to 70% of the laser power can be converted into Stokes. Since the infrared E_3 should be

generated simultaneously with the Stokes wave E_s, SPS can also be used to generate tunable coherent far-infrared generation. Using a 1-MW Q-switched ruby laser beam of about 2mm in diameter and a lens of 50 cm in focal length to focus the beam into a 3.3-cm a-axis $LiNbO_3$ crystal, Yarborough et al. [S.67] have detected a far-infrared output with a peak power of 5 watts and a tuning range from 50 to 238 cm^{-1}. Unfortunately, $LiNbO_3$ has a low damage threshold. A good single-mode laser should be used in order to avoid spatial inhomogeneity in the beam which increase the damage probability. Observation of far-infrared output by SPS in quartz has also been reported [S.68].

S.5 STIMULATED SPIN-FLIP RAMAN EMISSION

We have emphasized in the previous sections that the material excitations involved in SRS can also be electronic excitations. A case of special interest is SRS in n-type InSb by electrons making spin-flip transition. The corresponding Raman process is shown schematically in Fig. S.15.

Spontaneous spin-flip Raman scattering was first observed by Slusher et al. [S.69] following the theoretical predictions of Wolff [S.70] and Yafet [S.71]. Yafet showed that the Raman transition between the spin-up and spin-down states can be considered as a direct transition governed by an effective interaction Hamiltonian

$$\mathcal{H}'_{eff} \cong \left(\frac{e^2}{m_s c^2}\right) \left[\frac{E_g \hbar\omega_1}{E_g^2 - (\hbar\omega_1)^2}\right] \vec{\sigma} \cdot (\vec{A}_1 \times \vec{A}_2^*) \qquad \text{(S-46)}$$

where m_s is the spin mass which is related to the free electron mass m

and the spin g factor by $m_s = 2m/|g|$, E_g is the band gap, ω_1 is the incoming light frequency, $\vec{\sigma}$ is the spin operator, and $\vec{A}_1$ and $\vec{A}_2$ are the vector fields of the incoming and scattered radiation respectively. The spin-flip frequency or the Raman frequency shift is

$$\Delta\omega = 2\, g\mu_B B \tag{S-47}$$

where μ_B is the Bohr magneton and B is the applied magnetic field. From the first golden rule and Eq. (S-46), we find readily the spin-flip Raman cross-section as

$$(d\sigma/d\Omega)_{SF} \cong (e^2/m_s c^2)^2 (\omega_2/\omega_1)[E_g \hbar\omega_1/(E_g^2 - \hbar^2\omega_1^2)]^2 \tag{S-48}$$

for $\vec{A}_1$ perpendicular to $\vec{A}_2$.

In InSb, since $g \simeq 50$, we have $m_s \simeq 0.04\ m$ and if $E_g \hbar\omega_1 \approx (E_g^2 - \hbar^2\omega_1^2)$, $(d\sigma/d\Omega)_{SF}$ would be about 600 times larger than the Thomas scattering cross-section for free electrons. With resonant enhancement, $(d\sigma/d\Omega)_{SF}$ can be even much larger.

Using a CO_2 laser ($\omega_1 = 940\ cm^{-1}$), Slusher et al. [S.69] found experimentally in InSb $(d\sigma/d\Omega)_{SF} \simeq 10^{-23}\ cm^2/sr$ which agrees fairly well with the theoretical prediction from Eq. (S-48). With a CO laser ($\omega_1 = 1880\ cm^{-1}$ while $E_g/\hbar = 1900\ cm^{-1}$), Brueck and Mooradian [S.72] observed a strong resonant enhancement and found $(d\sigma/d\Omega)_{SF}$ can be 10^5 times larger than the Thomas cross-section (see Fig. S.16). The spin-flip Raman linewidth is also extremely narrow at low temperatures. Depending on the carrier concentration and $\vec{k}_s \cdot \vec{B}$ where $\vec{k}_s$ is the scattering wave vector, the

half width Γ can be as small as 0.15 cm^{-1} at $n = 1 \times 10^{16}$ cm^{-3}. [S.73].

The above spontaneous scattering data clearly suggest that spin-flip SRS can easily be seen in InSb. By assuming a Lorentzian Raman line with a half width $\Gamma = 2$ cm^{-1} and using Eq. (S-3) with $\rho_i - \rho_f = 1$, we find a spin-flip Raman gain $G_R = 1.7 \times 10^{-5}$ I cm^{-1} in an n-type InSb with $n = N = 3 \times 10^{16}$ cm^{-3}, where I is the CO_2 laser intensity in W/cm^2. [S.74]. As seen in Table S.1, this is the largest known Raman gain for all materials. The gain can be increased further by adjusting n appropriately with respect to Γ and by moving $\hbar\omega_1$ towards E_g. With a CO laser, G_R becomes 6×10^{-4} I cm^{-1} for the same n according to Eq. (S-48).

From the calculated gain, one expects that spin-flip SRS can be generated in InSb of few mm in length with a beam of $\sim 10^5$ W/cm^2 at 10.6 μm (CO_2 laser) or $\sim 10^3$ W/cm^2 at 5.3 μm (CO laser). Patel and Shaw [S.15] first observed spin-flip SRS in InSb using a Q-switched CO_2 laser at 10.6 μm as the pump. With an input peak power of 1 KW focused into an area of 10^{-3} cm^2 in a sample of $\sim$ 5 mm long and $n \approx 10^{16}$ cm^{-3} at $T \approx 18°K$, they obtained a Stokes peak power of 10 W. The Stokes frequency was tuned by an applied magnetic field according to Eq. (S-47). It was varied from 10.9 to 13.0 μm with B changing from 15 to 100 KG [S.74]. This then yields a practical tunable coherent source in the infrared. The Stokes output had a linewidth less than 0.03 cm^{-1} [S.74].

Breuck and Mooradian [S.75] found that spin-flip SRS in InSb could also be operated on the CW basis with a CO laser at 5.3 μm as the pump. Using a single-mode CO laser beam focused into an area of $\sim 5 \times 10^{-5}$ cm^2 in a 4.8-mm InSb with $n \approx 10^{16}$ cm^{-3} at $T \approx 30°K$, they obtained an SRS threshold of less than 50 mW, a power conversion efficiency of 50%, and

an output power in excess of 1 W. De Silets and Patel [S.76] have achieved a conversion efficiency of 80% with samples in a low magnetic field. The cw Stokes output can have a linewidth less than 1 KHz [S.77].

AntiStokes radiation and Stokes radiation up to the 4th order have been observed in the spin-flip Raman oscillator [S.75,76,78,79]. The antiStokes is generated through coupling to the Stokes (Section S.2.4) and the nth-order Stokes is generated by the (n-1)th-order Stokes (Section S.2.5).

The spin-flip transition can also be excited directly by an infrared wave through magnetic-dipole interaction. The interaction Hamiltonian for this direct process is

$$\mathcal{H}' = - g\mu_B \vec{\sigma} \cdot \vec{B}. \tag{S-49}$$

Since the spin-flip excitation can be excited by both the Raman process and direct absorption, we should in fact use the theory of stimulated polariton scattering in Section S.4 to describe the spin-flip SRS. In this case, the effective interaction energies $\langle \mathcal{H}^{(1)}_{eff} \rangle$ and $\langle \mathcal{H}^{NL}_{eff} \rangle$ in Eqs. (S-38) and (S-40) can be easily obtained from Eqs. (S-49) and (S-46), and hence A_{fi} and M_{fi} are readily known [S.16]. The solution in Eqs. (S-44,45) is then directly applicable to spin-flip SRS. In the present case, we always have $(\gamma_s + \gamma_3)^2 \gg \Lambda$ because the background absorption at ω_3 is strong. As a result, the stimulated polariton gain is almost exactly equal to the stimulated Raman gain assuming $\Lambda = 0$, as shown in Fig. S.17. We should, however, note that in stimulated polariton scattering, we expect to have the far-infrared generated together with

the Stokes. In Fig. S.17, we have also shown the ratio of the far-infrared output to the Stokes output for the collinear phase-mismatching case and for the non-collinear phase-matching case. The non-collinear phase-matching case appears to have a stronger far-infrared output.

No observation of direct far-infrared output from a spin-flip Raman oscillator has been reported yet, and only the collinear phase-nonmatching case has been tried [S.80]. However, by feeding both the laser and the Stokes into an InSb crystal, pulsed far-infrared output has been detected. Its maximum appears right at resonance [S.81]. The results agree very well with what the theory of stimulated polariton scattering would predict [S.16,82]. The far-infrared output from InSb can of course be tuned over the same frequency range as the Stokes [S.83]. This therefore gives us a potential far-infrared source which is intense, coherent, and tunable. It is possible that the cw spin-flip SRS can also lead to a cw tunable far-infrared source of extremely narrow linewidth.

S.6 TRANSIENT STIMULATED RAMAN SCATTERING

We have so far considered only the steady-state case of stimulated Raman emission. This is manifested by the time-independent wave equations we used in the theory. In the experiments, however, laser pulses are often used. Therefore, in general, we cannot neglect the time-dependence in the wave equations.

We can, however, still assume slow amplitude variation of the fields. The time-dependent wave equations corresponding to Eqs. (S-5, 29, 32) for infinite plane waves propagating along $\hat{z}$ in an isotropic medium are

$$\left(\frac{\partial}{\partial z} + \frac{1}{v_1}\frac{\partial}{\partial t}\right) \mathcal{E}_1(z,t) = i\left(\frac{2\pi\omega_1^2}{c^2 k_1}\right) N(M_{fi}^s)^* (\rho_i - \rho_f)\, \mathcal{E}_2 A$$

$$\left(\frac{\partial}{\partial z} + \frac{1}{v_s}\frac{\partial}{\partial t}\right) \mathcal{E}_s(z,t) = i\left(\frac{2\pi\omega_s^2}{c^2 k_s}\right) N M_{fi}^s (\rho_i - \rho_f)\, \mathcal{E}_1 A^*$$

$$\hbar(\partial/\partial t + \Gamma)A(z,t) = i M_{fi}^s \mathcal{E}_1 \mathcal{E}_s^* \qquad \text{(S-50)}$$

where $\mathcal{E}_1$ and $\mathcal{E}_2$ are defined in Eq. (S-4), A is defined through the relation $\psi = A \exp[i(k_1 - k_s)z - i\omega_{fi}t]$, $\omega_s = \omega_1 - \omega_{fi}$, v_1 and v_s are the group velocities at ω_1 and ω_s respectively.

Consider first the case where the amplitude variations of E_1 and E_s are sufficiently slow, so that $|\partial A/\partial t|$ is negligible compared with $|\Gamma A|$. Then, the material excitation $A(z,t) = i\, M_{fi}^s \mathcal{E}_1 \mathcal{E}_s^*/\hbar\Gamma$ follows almost instantaneously the time variation of $\mathcal{E}_1\mathcal{E}_s^*$. If the dispersion of the medium is also negligible, then $v_1 = v_s$. By transformation of variables $z' = z$ and $t' = t - z/v$, Eq. (S-50) reduces to

$$\partial\mathcal{E}_1/\partial z' = i(2\pi\omega_1^2/c^2 k_1)\, \chi_R^{(3)*} |\mathcal{E}_2|^2\, \mathcal{E}_1$$

$$\partial\mathcal{E}_s/\partial z' = i(2\pi\omega_s^2)/c^2 k_s)\, \chi_R^{(3)} |\mathcal{E}_1|^2\, \mathcal{E}_s$$

$$\chi_R^{(3)} = N|M_{fi}^s|^2(\rho_i - \rho_f)i\hbar\Gamma. \qquad \text{(S-51)}$$

These equations are identical to Eq. (S-7) except that $\mathcal{E}_1$ and $\mathcal{E}_s$ are now functions of z and $t - z/v$. In other words, $\mathcal{E}_1$ and $\mathcal{E}_s$ follow the steady-state variation in the retarded time coordinate. This is the

quasi-steady-state case. Using the retarded time, all our previous theoretical discussions are valid for this case.

For backward SRS, however, we should replace v_s in Eq. (S-50) by $-v_s$. The steady-state solution is no longer applicable unless the amplitude variations of the input pulses are negligible in a time which takes light to traverse the entire length of the medium. Maier et al. [S.50] have found the following general solution for this case (assuming $|v_1| = |v_s|$)

$$|\mathcal{E}_s|^2 \left(t+\frac{z}{v},\ t-\frac{z}{v}\right) = \frac{|\mathcal{E}_s|^2(t+z/v,0)}{F_s(t+z/v) + \exp[-F_1(t-z/v)]}$$

where

$$F_s(t+z/v) = \int_o^{t+z/v} g\ |\mathcal{E}_s(y,0)|^2 dy$$

$$F_1(t-z/v) = \int_o^{t-z/v} g\ |\mathcal{E}_1(0,y)|^2 dy$$

$$g = -\ (4\pi\omega_s^2/c^2k_s)\ \mathrm{Im}\chi_R^{(3)}. \qquad \text{(S-52)}$$

For given initial conditions at $z = 0$, one can then calculate the output Stokes intensity. An example is shown in Fig. S.18. It is seen that with a sufficiently long medium, the backward Stokes pulse is sharpened through amplification drastically. Physically, pulse sharpening occurs because the wavefront of the backward Stokes pulse continuously sees the fresh undepleted incoming laser beam and gets full amplification while the lagging part of the pulse does not. This phenomenon was actually observed in Kerr liquids where the initial Stokes pulse was generated by self-focusing at the end of the cell [S.50].

Consider next the case where $\mathcal{E}_1\mathcal{E}_s^*$ varies rapidly such that in Eq. (S-50) $|\partial A/\partial t|$ is no longer negligible compared with $|\Gamma A|$. This means that even the material excitation cannot reach its steady-state value during the pulse. Consequently, the forward Stokes generation also shows a transient behavior. This type of transient SRS occurs when the laser pulsewidth T_p is smaller than, or comparable with the dephasing time $T_2 = 1/\Gamma$ of the material excitation, or more rigorously, when $T_p < G_{Rm}\ell T_2$ where G_{Rm} is the steady-state Raman gain in Eq. (S-9) at the peak of the input pulse and ℓ is the length of the medium [S.84,85]. In gases, T_2 is of the order of 10^{-9} sec. or shorter. In liquids, T_2 is usually in the range of picoseconds. One must then use picosecond mode-locked pulses in general to study transient SRS, although Q-switched pulses may be used in some gas media [S.86]. With picosecond pulses, the backward Raman pulse intensity is hardly detectable because of the very limited interaction length with the incoming laser pulse. We can therefore limit our discussion to forward SRS only.

The theory of transient SRS has been discussed by many authors [S.85, 87-91]. It closely resembles the theory of transient stimulated Brillouin scattering [S.84]. Assume that both the depletion of laser power and the induced change of the population difference $(\rho_i - \rho_f)$ are negligible. Equation (S-50) then reduces to (assuming $v_1 = v_s$)

$$\left(\frac{\partial}{\partial z} + \frac{1}{v}\frac{\partial}{\partial t}\right)\mathcal{E}_s = i\,\eta_1\,\mathcal{E}_1(t-z/v)A^*$$

$$\left(\frac{\partial}{\partial t} + \Gamma\right)A^* = -\,i\,\eta_2\,\mathcal{E}_1^*(t-z/v)\mathcal{E}_s \qquad \text{(S-53)}$$

where

$$\eta_1 = (2\pi\omega_s^2/C^2k_s)\ N\ M_{fi}^s\ (\rho_i - \rho_f)$$

$$\eta_2 = (M_{fi}^s)^*/\hbar$$

and $\mathcal{E}_1(t-z/v)$ is prescribed by the initial condition.

Combining the two equations in Eq. (S-53) and using the new variables $z' = z$ and $t' = t - z/v$, we obtain a second-order partial differential equation [S.91]

$$[\partial^2/\partial t'\partial z' - \eta_1\eta_2|\mathcal{E}_1(t')|^2]\ U = 0 \qquad \text{(S-54)}$$

where $U = F\exp(\Gamma t')$ and F stands for either A^* or $\mathcal{E}_s$. By defining $\tau = \int_{-\infty}^{t'} |\mathcal{E}_1(t'')|^2 dt''$ as the integrated energy in the laser pulse up to t', the equation is further reduced to the standard form of a hyperbolic equation

$$(\partial^2/\partial\tau\partial z' - \eta_1\eta_2)U = 0$$

which can now be solved with arbitrary initial conditions. The solution takes the form [S.91],

$$\mathcal{E}_s(z',t') = \mathcal{E}_s(0,t') + (\eta_1\eta_2 z)^{1/2}\mathcal{E}_1(t')\int_{-\infty}^{t'} e^{-\Gamma(t'-t'')}$$

$$\times \{\mathcal{E}_1^*(t'')\, \mathcal{E}_s(0,t'')[\tau(t')-\tau(t'')]^{-1/2} I_1(2[\eta_1\eta_2(\tau(t')-\tau(t''))z']^{1/2})\}dt''$$

$$A^*(z',t') = i\eta_1\int_{-\infty}^{t'} e^{-\Gamma(t'-t'')}\{\mathcal{E}_1^*(t'')\, \mathcal{E}_s(0,t'')I_o(2[\eta_1\eta_2(\tau(t')-\tau(t''))z']^{1/2})\}dt'' \quad \text{(S-55)}$$

where the input conditions are $A^*(z') = 0$ at $t' \to -\infty$ and $\mathcal{E}_s(z',t') = \mathcal{E}_s(0,t')$ at $z = z' = 0$, and I_i is the ith order Bessel function of imaginary argument.

The Bessel functions have the asymptotic limits that $I_o(x) \cong 1$ and $I_1(x) \cong x$ for $x \ll 1$, and $I_i(x) \cong (2\pi x)^{-1/2}\exp(x)$ for $x \gg 1$. The Stokes amplitude therefore first increases linearly with z. Then, in the limit of large amplification, it varies exponentially in the form

$$\mathcal{E}_s(z',t') \propto \mathcal{E}_1(t')\int_{-\infty}^{t'} \mathcal{E}_1^*(t'')\mathcal{E}_s(0,t'')[\tau(t') - \tau(t'')]^{-1}$$

$$\times \exp\{-\Gamma(t'-t'') + 2[\eta_1\eta_2(\tau(t')-\tau(t''))z']^{1/2}\}. \quad \text{(S-56)}$$

For a rectangular laser pulse, it is easy to show from Eq. (S-56) that if the pulse is sufficiently long, then $\mathcal{E}_s$ takes on a steady-state exponential gain when $(t-t_o) > G_R z T_2$ where t_o is the starting time of the pulse. For this reason, T_p (pulsewidth) $< G_{Rm} z T_2$ is used as the condition for the occurrence of transient SRS as we mentioned before.

If $T_p < T_2$, the factor $\exp[-\Gamma(t'-t'')]$ can be neglected during the laser pulse. We can see from Eqs. (S-55,56) that the Stokes generated does not grow appreciably at the leading edge of the laser pulse, but increases rapidly towards the middle part.

It finally drops off following the laser pulse shape at the tail. Therefore, the Stokes peak always appears after the laser peak and the Stokes pulse should be narrower than the laser pulse. The material excitation behaves in a similar manner, but towards the tail it decays exponentially as $\exp(-\Gamma t)$ even after the laser intensity has dropped to almost zero. In the limit of large amplification, we have from Eq. (S-56) [S.91]

$$(\mathcal{E}_s)_{max} \propto \exp(G_T z/2) \tag{S-57}$$

where the transient gain G_T is given by

$$G_T \simeq 4\,[\eta_1\eta_2 \langle|\mathcal{E}_1|^2\rangle T_P/z]^{1/2}$$

$$\langle|\mathcal{E}_1|^2\rangle T_P \equiv \int_{-\infty}^{\infty} |\mathcal{E}_1(t)|^2 dt.$$

This transient gain is then independent of the laser pulse shape. For a pulse of the form $\mathcal{E}_1(t') = \mathcal{E}_{1m} \exp(-|t'/T|^n)$, it has been shown [S.91] that the peak of the Stokes pulse is delayed from the laser peak by a time $t_D = T(\frac{1}{2} \log G_{Rm} z)^{1/n}$.

Carman et al.[S.91] have carried out numerical calculations of transient SRS for various pulse shapes. Their results of $G_T z$ for Gaussian laser input pulses of different pulsewidths versus the maximum steady-state gain $G_{mR} z$ are presented in Fig. S.19. It shows that when $T_P > G_{Rm} z T_2$, we have $G_T \simeq G_{Rm}$, and otherwise, $G_T < G_{Rm}$ as the transient gain should be. At sufficiently large $G_{Rm} z$, the curves also show a $z^{1/2}$ dependence for $G_T z$ as predicted by Eq. (S-57). The variation of the time delay t_D with

G_T for Gaussian laser pulses of different pulse widths is shown in Fig. S.20. As expected, t_D increases with G_T, more rapidly at large values of G_T. In Fig. S.20, sharpening of the Stokes pulse with increasing G_T is also shown. The effects of phase modulation and linear dispersion have also been studied [S.91].

Earlier experiments by Hagenlocker et al. [S.86] first suggested the transient behavior of SRS in gases with Q-switched laser pulses. Later, with picosecond mode-locked pulses, transient effects of SRS in liquids were observed [S.92-97]. Since the transient gain G_T depends only on the total Raman cross-section ($\propto \eta_1\eta_2$) while the steady-state gain G_{Rm} is also inversely proportional to the linewidth Γ, it is possible to observe in transient SRS some Raman modes which are not observed in steady-state SRS [S.96]. More than one Raman mode can show up in transient SRS [S.96,98]. Carman and Mack [S.99] have recently made quantitative measurements on transient SRS in SF_6 gas. They chose SF_6 because of its small linear dispersion and/or the absence of other nonlinear effects during SRS. Their results agree well with the predictions of the theory. A better experiment to test the theory of transient SRS is, however, to measure the temporal variation of Stokes amplification in an amplifier cell as we discussed earlier in Section S.3.2. Such an experiment, however, has not yet been carried out.

S.7 APPLICATIONS OF STIMULATED RAMAN SCATTERING

We have seen how SRS can be used to generate coherent light at new frequencies. There are a number of other applications of SRS. We shall discuss only a few of them in the following.

S.7.1 MEASUREMENTS OF VIBRATIONAL LIFETIMES

In analogy to the magnetic resonance case, there are two characteristic lifetimes for each molecular or lattice vibration: the longitudinal lifetime T_1 and the transverse (or dephasing) lifetime T_2 [S.34]. These lifetimes cannot be obtained simply from linewidth measurements. Only in the limit of homogeneous broadening is T_2 equal to the inverse halfwidth, but even then T_2 can be very different from T_1. The two lifetimes can, however, be measured directly by watching the vibrational decay after a short pulse excitation. Both the pulse excitation and the monitoring of vibrational decay can be achieved through Raman transitions. In the case of condensed matter, the vibrational lifetimes are often in the picosecond range. Then, the SRS method appears to be the only way to measure the vibrational lifetimes directly.

As discussed in Section S.2 and S.6, the time-dependent excitation of the coherent vibrational field and the population of excited molecular vibration is governed by the following set of equations (from Eqs. (S-50), (S-24), and (S-25))

$$\left(\frac{\partial}{\partial z} + \frac{1}{v_1}\frac{\partial}{\partial t}\right)\mathcal{E}_1(z,t) = i\left(\frac{2\pi\omega_1^2}{c^2 k_1}\right)N\left(\frac{2\omega_o}{\hbar}\right)^{1/2}(M_{fi}^s)^*(\rho_i - \rho_f)\mathcal{E}_s Q$$

$$\left(\frac{\partial}{\partial z} + \frac{1}{v_s}\frac{\partial}{\partial t}\right)\mathcal{E}_s(z,t) = i\left(\frac{2\pi\omega_s^2}{c^2 k_s}\right)N\left(\frac{2\omega_o}{\hbar}\right)^{1/2}M_{fi}^s(\rho_i - \rho_f)\mathcal{E}_1 Q^*$$

$$\left(\frac{\partial}{\partial t} + \frac{1}{T_2}\right)Q(z,t) = iM_{fi}^s(2\hbar\omega_o)^{-1/2}\mathcal{E}_1\mathcal{E}_s^*$$

$$\left(\frac{\partial}{\partial t} + \frac{1}{T_1}\right)\Delta\rho = \frac{iN}{2\hbar}\left(\frac{2\omega_o}{\hbar}\right)^{1/2}[M_{fi}\mathcal{E}_1\mathcal{E}_s^* Q^* - M_{fi}^*\mathcal{E}_1^*\mathcal{E}_2 Q](\rho_i - \rho_f)$$

$$\rho_i - \rho_f = \rho_i^o - \rho_f^o - 2\Delta\rho. \qquad \text{(S-58)}$$

We assume that the experiment is designed to have negligible depletion of the $\mathcal{E}_1$ field and $\Delta\rho \ll (\rho_i^o - \rho_f^o)$. Thus, with $\mathcal{E}_1$ = constant and $(\rho_i - \rho_f)$ replaced by $(\rho_i^o - \rho_f^o)$, the solution for $\mathcal{E}_s(z,t)$ and $Q(z,t)$ is just the transient solution discussed in the previous section [S.91]. The solution for $\Delta\rho(z,t)$ is then obtained by solving the equation of $\Delta\rho$ with the calculated $\mathcal{E}_s(z,t)$ and $Q(z,t)$. The temporal behavior of both Q and $\Delta\rho$ can be monitored experimentally by a probing beam. The coherent vibrational field Q should scatter the probing beam coherently in the phase-matched direction. The population change $\Delta\rho$ gives rise to a change in the intensity of the incoherent Stokes and antiStokes scattering.

However, since T_1 and T_2 of condensed matter are in the picosecond range, it is difficult to monitor the continuous variation of scattering of the probing beam with time electronically. We must resort to optical means with the help of picosecond pulses. We can use a picosecond pulse at ω_1 to excite the vibration via Stokes transition and then another picosecond pulse at ω_2, time-delayed by t_D from the first pulse, to probe Q and $\Delta\rho$ via antiStokes scattering. For the coherent antiStokes scattering in the phase-matching direction, the antiStokes field $\mathcal{E}_a(z,t)$ at frequency $\omega_2 + \omega_o$ obeys the equation (see Section S.2)

$$\left(\frac{\partial}{\partial z} + \frac{1}{v_a}\frac{\partial}{\partial t}\right)\mathcal{E}_a(z,t) = i\left(\frac{2\pi\omega_a^2}{c^2 k_a}\right)N\left(\frac{2\omega_o}{\hbar}\right)^{1/2}(M_{fi}^a)^*(\rho_i^o-\rho_f^o)\mathcal{E}_2(z,t)Q(z,t+t_D) \qquad \text{(S-59)}$$

where $\mathcal{E}_2$ is the probing pulse field, and the nonresonant contribution to the nonlinear polarization is neglected. The antiStokes output from the medium as a function of the time delay t_D is given by

$$S^{coh}(t_D) \propto \int |\mathcal{E}_a(\ell, t' = t - z/v)|^2 dt'$$

$$= (\text{Constant}) \int dt' \left| \int dz \mathcal{E}_2(z,t') Q(z,t'+t_D) \right|^2. \qquad \text{(S-60)}$$

The incoherent antiStokes scattering gives a signal

$$S^{inc}(t_D) = (\text{Constant}) \int dt\, dz \;\; |\mathcal{E}_2(z,t)|^2 \Delta\rho(z,t + t_D). \qquad \text{(S-61)}$$

Knowing the exciting and probing pulses, and the solution for $Q(z,t')$ in Eq. (S-55) (replacing A by $(2\omega_o/\hbar)^{1/2}Q$), we can then calculate S^{coh} and S^{inc} from the above equations. It can be shown from Eq. (S-55) that if the exciting pulse has a pulsewidth T_p smaller than or comparable with T_2, then $Q(z,t)$ will show an exponential decay $\exp(-t/T_2)$ at large t, or $S^{coh}(t_D) \propto \exp(-t_D/T_2)$ for $t_D \gg T_2$. Similarly, from the equation for $\Delta\rho$ in Eq. (S-58), we realize that $\Delta\rho(z,t)$ or $S^{inc}(t_D)$ will show an exponential decay tail with a time constant T_1. Thus, if $T_p \lesssim T_1, T_2$, then we can obtain T_1 and T_2 directly by measuring the exponential decays of $S^{coh}(t_D)$ and $S^{inc}(t_D)$.

DeMartini and Ducuing [S.100] first used such a method to measure T_1 of the 4155 cm^{-1} vibrational excitation of gaseous H_2. In this case, T_1 is about 30 μsec at 0.03 atmospheric pressure. Ultrashort laser pulses are not needed for the measurements. Recently, Alfano and Shapiro [S.101] and Kaiser and his associates [S.102-105] have used picosecond mode-locked laser pulses to measure T_1 and T_2 of molecular or lattice vibration in liquids and solids. One of their experimental arrangements is shown in Fig. S.21. The mode-locked pulse from a Nd glass laser is

used to excite the vibration by SRS, and the second-harmonic of the mode-locked pulse is used to probe the vibrational excitation. An example of their results is shown in Fig. S.22. The exponential tails of the $S^{inc}(t_D)$ and $S^{coh}(t_D)$ curves in the figure yield T_1 and T_2 readily. These were the first direct measurements of vibrational relaxation times in condense matter. The same technique can of course be applied to the measurements of relaxation times of other types of excitations. By detecting the incoherent antiStokes signal at various frequencies ω_a as a function of t_D, one can also study the decay routes of a particular excitation [S.106,107].

S.7.2 MEASUREMENTS OF THIRD-ORDER NONLINEAR SUSCEPTIBILITIES

Consider now the steady-state case where the material excitation ψ with a resonant frequency ω_o is driven by the incoming fields E_1 and E_s at ω_1 and ω_s respectively. A third incoming field E_2 at ω_2 is then used to probe ψ and the coherent antiStokes scattering at $\omega_a = \omega_1 - \omega_s + \omega_2$ is detected. From the discussion in Section S.2.4, the antiStokes field E_a obeys the equation

$$\frac{\partial \mathcal{E}_a}{\partial z} = i\left(\frac{2\pi\omega_a^2}{c^2 k_{az}}\right) \chi^{(3)} \; \mathcal{E}_2 \mathcal{E}_1 \mathcal{E}_s^* \; e^{i\Delta k_z z} \tag{S-62}$$

where

$$\Delta\vec{k} = \vec{k}_1 + \vec{k}_2 - \vec{k}_s$$

$$\chi^{(3)} \equiv \hat{e}_a \cdot \overleftrightarrow{\chi}^{(3)} : \hat{e}_2 \hat{e}_1 \hat{e}_s = \chi_R^{(3)} + \chi_{NR}^{(3)}$$

$$\chi_R^{(3)} = N \, M_{fi}^{s} (M_{fi}^{a})^* (\rho_i^o - \rho_f^o)/\hbar(\omega_1 - \omega_s - \omega_o + i\Gamma)$$

and $\chi^{(3)}_{NR}$ is the nonresonant contribution to $\chi^{(3)}$. At phase matching $\Delta k = 0$, the antiStokes output is given by

$$|\mathcal{E}_a|^2 = \left(\frac{2\pi\omega_a^2}{2k_{az}}\right)^2 |\chi^{(3)}|^2 |\mathcal{E}_1|^2 |\mathcal{E}_2|^2 |\mathcal{E}_s|^2. \tag{S-63}$$

With the incoming beam intensities kept constant, $|\mathcal{E}_a|^2$ as a function of $\omega_1 - \omega_s$ is a maximum when $|\chi^{(3)}|$ is a maximum.

If the ω_o resonance is a narrow one, and the other resonances are far away, the dispersion of $\chi^{(3)}_{NR}$ is negligible when $\omega_1 - \omega_s$ varies around ω_o over a few linewidths. Then, we can easily show from Eq. (S-62) that the maximum and minimum of $|\chi^{(3)}|$ occur at $(\omega_1 - \omega_s)_+$ and $(\omega_1 - \omega_s)_-$ respectively with

$$(\omega_1 - \omega_s)_\pm = \omega_o + \frac{1}{2}\left\{-\frac{a}{\chi^{(3)}_{NR}}\right) \pm \left[\left(\frac{a}{\chi^{(3)}_{NR}}\right)^2 + \Gamma^2\right]^{1/2} \tag{S-64}$$

where

$$a = N M^s_{fi} (M^a_{fi})^* (\rho^o_i - \rho^o_f)/\hbar$$

such that $\chi^{(3)}_R = a/(\omega_1 - \omega_s - \omega_o + i\Gamma)$. An example of $|\chi^{(3)}_R|$ versus $(\omega_1 - \omega_s)$ around ω_o is shown in Fig. S.23. From Eq. (S-64), we have

$$(\omega_1 - \omega_s)_+ + (\omega_1 - \omega_s)_- = 2\omega_o - a/\chi^{(3)}_{NR}$$

$$[(\omega_1 - \omega_s)_+ - (\omega_1 - \omega_s)_-]^2 = (a/\chi^{(3)}_{NR})^2 + \Gamma^2. \tag{S-65}$$

In many cases where $|a/\chi^{(3)}_{NR}| \gg \Gamma$, the maximum of $|\chi^{(3)}|$ appears at $\omega_1 - \omega_s = \omega_o$, and then from Eq. (S-65) we can find $a/\chi^{(3)}_{NR}$ and Γ by

measuring $(\omega_1 - \omega_s)_{\pm}$. We can of course obtain ω_o and Γ easily from spontaneous Raman scattering data. The interesting thing here is that we can now obtain $a/\chi_{NR}^{(3)}$ directly from frequency measurements, and with a deduced from the spontaneous Raman cross-section we can find $\chi_{NR}^{(3)}$. If the particular Raman mode is far away from other modes, then $\chi_{NR}^{(3)}$ is mainly due to electronic contribution. We can also obtain $\chi_{NR}^{(3)}$ by measuring the absolute intensity of the coherent antiStokes signal, but it is well known that frequency measurements should be much more accurate than absolute intensity measurements.

This type of wave-mixing experiments has been carried out with $\omega_1 - \omega_s$ around Raman-active vibrational modes in various materials by Wynne [S.108,109] and by Bloembergen and his associates [S.110-113]. More recently, using this method, Levenson [S.112] and Levenson and Bloembergen [S.113] have measured $\chi_{NR}^{(3)}$ for a large number of liquids and solids. Their experimental setup is shown in Fig. S.24. Two N_2-laser-pumped dye lasers were used as the tunable sources. Their result on calcite is shown in Fig. S.23 as an example. When there are several Raman-active modes close together, the analysis becomes somewhat more complicated, but it is clear that with the help of the spontaneous Raman scattering data, we can still deduce $\chi_{NR}^{(3)}$ from the wave-mixing results [S.113]. In a crystal with no inversion symmetry, the modes can be both Raman active and infrared active. The coupled infrared and material excitational wave (or the polariton wave) discussed in Section S.4 must now be used instead of ψ in the above formalism. In addition, the field at $\omega_a = \omega_1 - \omega_s + \omega_2$ can also be generated by another two-step process in which the sum-frequency field $E(\omega_1 + \omega_2)$ is first created and then mixed

with $E^*(\omega_s)$ to produce $E(\omega_a)$. The analysis for this case is more complicated but quite straightforward [S.111,114]. Interference between various contributions to E_a can be observed in the dispersion measurements [S.111]. We note again that the above analysis is applicable to any material excitation such as magnon, plasmon, etc., although experiments so far have only been performed on Raman-active vibrational modes.

S.7.3 DETECTION OF LOW-CONCENTRATION SUBSTANCES

As is well known, Raman modes can be used to identify a substance. Likewise, the resonant curve of $|\chi^{(3)}|$ or $|E_a|^2$ in Eq. (S-63) can be used to identify a substance or to detect low-concentration substances in a mixture as long as $|\chi_R^{(3)}|_{max} \gtrsim |\chi_{NR}^{(3)}|$ in Eq. (S-62). This latter technique is most useful in gas mixtures where the Raman linewidths can be very narrow and consequently, $|\chi_R^{(3)}|_{max}$ can be quite large even for low concentrations (see Eq. (S-62)). Régnier and Taran [S.115] have shown that with input laser powers of about 1 Mwatt, they can detect a H_2 concentration of about 10 ppm in N_2 gas of 1 atm. pressure. For comparison, the 100 ppm H_2-in-N_2 mixture yields roughly 1 Watt of coherent antiStokes signal from 1-Mwatt input laser pulses, while spontaneous scattering from the same focal volume with 1 Mwatts of laser power would lead to an incoherent Stokes emission of 10^{-10} watt per solid angle. The detection sensitivity can of course be greatly improved by letting ω_1 or ω_2 approach electronic resonances. Through the resonant enhancement in M_{fi} in Eq. (S-1), $|\chi_R^{(3)}|$ for a gas substance can increase by five to six orders of magnitude. This technique can be used to study the gas mixture in a flame, in a combustion engine, or in a supersonic jet flow [S.115]. Presumably, it can also be

used to monitor the polluting substances in a smoke stack and automobile exhaust.

S.7.4 OTHER MISCELLANEOUS APPLICATIONS

Plasma waves as a material excitation can be excited by SRS [S.36,116]. The excited plasma waves will of course be damped with the energy turned into heat. This has been proposed as a possible means of heating a plasma for controlled fusion work [S.117]. However, no clean SRS experiment on plasma has yet been reported.

The stimulated antiStokes absorption (Section S.3.4). often known as the inverse Raman effect, leads to a new Raman spectroscopic technique [S.59, 118, 119]. By shining a laser pulse and a pulse of continuous spectrum simultaneously on a sample, the Raman spectrum can be obtained in one shot. More recently, the technique has been extended to the picosecond regime with the use of mode-locked pulses [S.120].

SRS is one of these effects which limit the propagation of high-intensity laser beams in materials. It is particularly important for high-intensity beam propagation in air for optical communications or other purposes. We have seen in Eqs. (S-2,3) that the Raman gain G_R is proportional to $\omega_2|M_{fi}|^2|E_1|^2$ where $|M_{fi}|^2$ usually increases as ω_1 increases. Consequently, SRS is often weaker at lower frequencies. Therefore, in order to transmit a high-power laser beam through a material, one should reduce G_R by using a larger beam size and a lower frequency.

S.8 CONCLUDING REMARKS

Because of limitation of space, we have omitted the discussion on

a number of topics in SRS. We have not discussed the tensorial form of the Raman susceptibility $\overleftrightarrow{\chi}_R^{(3)}$ with respect to the symmetry of the medium and its tensorial relation with the spontaneous Raman cross-section $d\overleftrightarrow{\sigma}/d\Omega$. We have not considered SRS in anisotropic crystals [S.121]. We have not mentioned SRS in optical waveguides [S.122]. We also have not discussed resonant SRS [S.123]. The latter case is particularly interesting in alkali vapor systems [S.124,125]. Resonant SRS has recently been used to facilitate generation of tunable infrared [S.126] and tunable vacuum ultraviolet [S.127] by optical mixing in alkali vapor.

In conclusion, we believe the physics of SRS is basically understood. In actual experiments, the results of SRS may be complicated by other competing nonlinear optical effects. Influence of other nonlinear effects on SRS and vice versa are also qualitatively understood in most cases, but quantitative analysis is often quite difficult. SRS has already been used in a number of applications. With the recent advance of tunable lasers, it is expected that more research on resonant SRS will be carried out in the near future.

This paper supported in part by the U.S. Atomic Energy Commission.

REFERENCES

S.1 See, for example, W. Heitler, The Quantum Theory of Radiation (Cambridge University Press, New York, 3d Ed., 1954) p. 192.

S.2 R. Glauber, Phys. Rev. 130, 2529 (1963); 131, 2766 (1963).

S.3 R. W. Hellwarth, Phys. Rev. 130, 1850 (1963); Appl. Optics 2, 847 (1963).

S.4 E. J. Woodbury and W. K. Ng, Proc. IRE 50, 2347 (1962).

S.5 G. Eckardt, R. W. Hellwarth, F. J. McClung, S. E. Schwartz, D. Weiner, and E. J. Woodbury, Phys. Rev. Letters 9, 455 (1962).

S.6 M. Geller, D. P. Bortfeld, and W. R. Sooy, Appl. Phys. Letters 3, 36 (1963).

S.7 B. P. Stoicheff, Phys. Letters 7, 186 (1963).

S.8 G. Eckardt, D. P. Bortfeld, and M. Geller, Appl. Phys. Letters 3, 137 (1963).

S.9 R. W. Minck, R. W. Terhune, and W. G. Rado, Appl. Phys. Letters 3, 181 (1963).

S.10 R. W. Terhune, Solid State Design 4, 38 (1963).

S.11 H. J. Zeiger and P. E. Tannenwald, Proceedings of the Third International Conference on Quantum Electronics, Paris, 1963, edited by P. Grivet and N. Bloembergen (Columbia University Press, New York, 1964) p. 1589.

S.12. R. Y. Chiao and B. P. Stoicheff, Phys. Rev. Letters 12, 290 (1964).

S.13 S. K. Kurtz and J. A. Giordmaine, Phys. Rev. Letters 22, 192 (1969).

S.14 J. Gelbwachs, R. H. Pantell, H. E. Puthoff, and J. M. Yarborough, Appl. Phys. Letters 14, 258 (1969).

S.15 C. K. N. Patel and E. D. Shaw, Phys. Rev. Letters 24, 451 (1970).

S.16 Y. R. Shen, Appl. Phys. Letters 23, 516 (1973).

S.17 S. L. Shapiro, J. A. Giordmaine, and K. W. Wecht, Phys. Rev. Letters 19, 1093 (1967).

S.18 See, for example, C. S. Wang, Phys. Rev. 182, 482 (1969).

S.19 D. Von der Linde, A. Laubereau, and W. Kaiser, Phys. Rev. Letters 26, 954 (1971).

S.20 R. R. Alfano and S. L. Shapiro, Phys. Rev. Letters 26, 1247 (1971).

S.21 J. A. Armstrong, N. Bloembergen, J. Ducuing, and P. S. Pershan, Phys. Rev. 127, 198 (1962).

S.22 Y. R. Shen and N. Bloembergen, Phys. Rev. 137, A1786 (1965).

S.23 N. Bloembergen, Am. J. Phys. 35, 989 (1967).

S.24 W. Kaiser and M. Maier, in Laser Handbook, ed. by F. T. Arecchi and E. O. Schulz-Dubois (North-Holland Publishing Co., Amsterdam, 1972) p. 1077.

S.25 M. Sparks, Phys. Rev. Letters 32, 450 (1974).

S.26 E. Garmire, E. Pandarese, and C. H. Townes, Phys. Rev. Letters 11, 160 (1963).

S.27 N. Bloembergen and Y. R. Shen, Phys. Rev. Letters 12, 504 (1964).

S.28 V. T. Platonenko and R. V. Khokhlov, Soviet Physics JETP 19, 378, 1435 (1964).

S.29 C. L. Tang and T. F. Deutsch, Phys. Rev. 138, A1 (1965).

S.30 H. Haus, P. L. Kelley, and H. Zeiger, Phys. Rev. 138, A690 (1965).

S.31 See, for example, N. Bloembergen, Nonlinear Optics (W. A. Benjamin, Inc., New York, 1965).

S.32 N. Bloembergen and Y. R. Shen, Phys. Rev. 133, A37 (1964).

S.33 See, for example, Ref. [S.31], p. 27.

S.34 See, for example, A. Abragam, Principles of Nuclear Magnetism (Oxford University Press, Oxford, 1961); P. S. Hubbard, Rev. Mod. Phys. 33, 249 (1961).

S.35 Y. R. Shen and N. Bloembergen, Phys. Rev. 143, 372 (1966).

S.36 N. Bloembergen and Y. R. Shen, Phys. Rev. 141, 298 (1966).

S.37 R. Loudon, Proc. Phys. Soc. 82, 393 (1963); P. N. Butcher, R. Loudon, and T. P. McLean, Proc. Phys. Soc. 85, 565 (1965).

S.38 D. Fröhlich, E. Mohler, and P. Wiesner, Phys. Rev. Letters 26, 554 (1971).

S.39 D. C. Haueisen and H. Mahr, Phys. Rev. Letters 26, 838 (1971); Phys. Rev. B8, 2969 (1973).

S.40 D. Boggett and R. Loudon, Phys. Rev. Letters 28, 1051 (1972).

S.41 R. Y. Chiao, C. H. Townes, and B. P. Stoicheff, Phys. Rev. Letters 12, 592 (1964).

S.42 D. Von der Linde, M. Maier, and W. Kaiser, Phys. Rev. 178, 11 (1969).

S.43 F. J. McClung, W. G. Wagner, and D. Weiner, Phys. Rev. Letters 15, 96 (1965); G. Bret, Comptes Rendus 259, 2991 (1964); 260, 6323 (1965).

S.44 B. P. Stoicheff, Phys. Letters 7, 186 (1963).

S.45 R. W. Terhune, Solid State Design 4, 38 (1964); H. J. Zeiger, P. E. Tannenwald, S. Kern, and R. Hurendeen, Phys. Rev. Letters 11, 419 (1963); E. Garmire, Physics of Quantum Electronics, ed. by P. L. Kelley, B. Lax, and P. E. Tannenwald, (McGraw-Hill

Book Co., New York, 1966) p. 167; E. Garmire, Phys. Letters 17, 251 (1965).

S.46 G. Hauchecorne and G. Mayer, Comptes Rendus 261, 4014 (1965); Y. R. Shen and Y. J. Shaham, Phys. Rev. Letters 15, 1008 (1965); P. Lallemand and N. Bloembergen, Phys. Rev. Letters 15, 1010 (1965).

S.47 P. L. Kelley, Phys. Rev. Letters 15, 1005 (1965).

S.48 C. C. Wang, Phys. Rev. Letters 16, 344 (1966).

S.49 M. M. T. Loy and Y. R. Shen, Appl. Phys. Letters 19, 285 (1971).

S.50 M. Maier, W. Kaiser, and J. A. Giordmaine, Phys. Rev. 177, 580 (1969); Phys. Rev. Letters 17, 1275 (1966).

S.51 Y. R. Shen and M. M. T. Loy, Phys. Rev. A3, 2099 (1971); G. K. L. Wong and Y. R. Shen, Appl. Phys. Letters 21, 163 (1972).

S.52 N. Bloembergen and P. Lallemand, Phys. Rev. Letters 16, 81 (1966).

S.53 A. Penzkofer, A. Laubereau, and K. Kaiser, Phys. Rev. Letters 31, 863 (1973).

S.54 C. A. Sacchi, C. H. Townes, and J. R. Lifshitz, Phys. Rev. 174, 439 (1968).

S.55 J. B. Grun, A. K. McQuillan, and B. P. Stoicheff, Phys. Rev. 180, 61 (1969).

S.56 J. H. Dennis and P. E. Tannenwald, Appl. Phys. Letters 5, 58 (1964); H. Takuma and D. A. Jennings, Appl. Phys. Letters 4, 185; 5, 239 (1964).

S.57 N. Bloembergen, G. Bret, P. Lallemand, A. Pine, and P. Simova, IEEE J. Quantum Electron. 3, 197 (1967); P. Lallemand, P. Simova, and G. Bret, Phys. Rev. Letters 17, 1239 (1966).

S.58 N. Bloembergen and P. Lallemand, Physics of Quantum Electronics edited by P. L. Kelley, B. Lax, and P. E. Tannenwald, (McGraw-Hill Book Co., New York, 1966) p. 137.

S.59 W. J. Jones and B. P. Stoicheff, Phys. Rev. Letters 13, 657 (1964); A. K. McQuillan and B. P. Stoicheff, Physics of Quantum Electronics, edited by P. L. Kelley, B. Lax, and P. E. Tannenwald (McGraw-Hill Book Co., New York, 1966) p. 192.

S.60 K. Huang, Nature 167, 779 (1951); Proc. Roy. Soc. (London), A208, 352 (1951); M. Born and K. Huang, Dynamical Theory of Crystal Lattices (Oxford University Press, London, 1954), chapter II.

S.61 J. J. Hopfield, Phys. Rev. 112, 1555 (1958).

S.62 Y. R. Shen, Phys. Rev. 138, A1741 (1965).

S.63 C. H. Henry and C. G. B. Garrett, Phys. Rev. 171, 1058 (1968).

S.64 H. E. Puthoff, R. H. Pantell, and B. G. Huth, J. Appl. Phys. 37, 860 (1966); F. De Martini, J. Appl. Phys. 37, 4503 (1966); B. A. Akanev, S. A. Akhmanov, and Yu. G. Khronopulo, Sov. Phys. JETP 28, 656 (1969).

S.65 See, for example, N. Bloembergen, Nonlinear Optics (W. A. Benjamin, Inc., New York, 1965) sec. 4.4

S.66 S. S. Sussman, Microwave Lab. Report No. 1851, Stanford University (1970).

S.67 J. M. Yarborough, S. S. Sussman, H. E. Puthoff, R. H. Pantell, and B. C. Johnson, Appl. Phys. Letters 15, 102 (1969).

S.68 S. Biraud-Laval and G. Chartier, Phys. Letters 30A, 177 (1969).

S.69 R. E. Slusher, C. K. N. Patel, and P. A. Fleury, Phys. Rev. Letters 18, 77 (1967).

S.70 P. A. Wolff, Phys. Rev. Letters 16, 225 (1966).

S.71 Y. Yafet, Phys. Rev. 152, 858 (1966).

S.72 S. R. J. Brueck and A. Mooradian, Phys. Rev. Letters 28, 161 (1972).

S.73 S. R. J. Brueck and A. Mooradian, Phys. Rev. Letters 28, 1458 (1972).

S.74 C. K. N. Patel and E. D. Shaw, Phys. Rev. B3, 1279 (1971).

S.75 A. Mooradian, S. R. J. Brueck, and F. A. Blum, Appl. Phys. Letters 17, 481 (1970); S. R. J. Brueck and A. Mooradian, Appl. Phys. Letters 18, 229 (1971).

S.76 C. S. DeSilets and C. K. N. Patel, Appl. Phys. Letters 22, 543 (1973).

S.77 C. K. N. Patel, Phys. Rev. Letters 28, 649 (1972).

S.78 E. D. Shaw and C. K. N. Patel, Appl. Phys. Letters 18, 215 (1971).

S.79 C. K. N. Patel, Appl. Phys. Letters 18, 274 (1971).

S.80 V. T. Nguyen and T. J. Bridges, Proceedings of the Laser Spectroscopy Conference, Vail, Colorado, June 1973 (to be published).

S.81 V. T. Nguyen and T. J. Bridges, Phys. Rev. Letters 29, 359 (1972).

S.82 T. L. Brown and P. A. Wolff, Phys. Rev. Letters 29, 362 (1972).

S.83 T. J. Bridges and V. T. Nguyen, Appl. Phys. Letters 23, 107 (1973).

S.84 N. M. Kroll, J. Appl. Phys. 36, 34 (1965).

S.85 C. S. Wang, Phys. Rev. 182, 482 (1969).

S.86 E. E. Hagenlocker, R. W. Minck, and W. G. Rado, Phys. Rev. 154, 226 (1967).

S.87 S. A. Akhmanov, Mat. Res. Bull. 4, 455 (1969).

S.88 S. A. Akhmanov, A. P. Sakhorukov, and A. S. Chirkin, Zh ETF 55, 143 (1968) [Translation: Sov. Phys. JETP 28, 748 (1969)].

S.89 T. I. Kuznetsova, Zh ETF Pis'ma 10, 153 (1969) [(Translation: Sov. Phys. JETP Lett. 10, 98 (1969)].

S.90 N. M. Kroll and P. L. Kelley, Phys. Rev. A4, 763 (1971).

S.91 R. L. Carman, F. Shimizu, C. S. Wang, and N. Bloembergen, Phys. Rev. A2, 60 (1970).

S.92 S. L. Shapiro, J. A. Giordmaine, and K. W. Wecht, Phys. Rev. Letters 19, 1093 (1967).

S.93 G. Bret and H. Weber, IEEE J. Quant. Electron. QE-4, 807 (1968).

S.94 M. J. Colles, Optics Comm. 1, 169 (1969).

S.95 M. A. Bolshov, Yu. I. Golyaev, V. S. Dneprovskii, and I. I. Nurminskii, Zh ETF 57, 346 (1969) [Translation: Sov. Phys. JETP 30, 190 (1970)].

S.96 R. L. Carman, M. E. Mack, F. Shimizu, and N. Bloembergen, Phys. Rev. Letters 23, 1327 (1969).

S.97 M. J. Colles, G. E. Walrafen, and K. W. Wecht, Chem. Phys. Letters 4, 621 (1970).

S.98 M. E. Mack, R. L. Carman, J. Reintjes, and N. Bloembergen, Appl. Phys. Letters 16, 209 (1970).

S.99 R. L. Carman and M. E. Mack, Phys. Rev. A5, 341 (1972).

S.100 F. De Martini and J. Ducuing, Phys. Rev. Letters 17, 117 (1966).

S.101 R. R. Alfano and S. L. Shapiro, Phys. Rev. Letters 26, 1247 (1971).

S.102 D. von der Linde, A. Laubereau, and W. Kaiser, Phys. Rev. Letters 26, 954 (1971).

S.103 A. Laubereau, D. von der Linde, and W. Kaiser, Phys. Rev. Letters 27, 802 (1971).

S.104 A. Laubereau, D. von der Linde, and W. Kaiser, Phys. Rev. Letters 28, 1162 (1972).

S.105 A. Laubereau, D. von der Linde, and W. Kaiser, Optics Comm. 7, 173 (1973).

S.106 R. R. Alfano and S. L. Shapiro, Phys. Rev. Letters 29, 1655 (1972).

S.107 A. Laubereau, D. von der Linde, and W. Kaiser (to be published).

S.108 J. J. Wynne, Phys. Rev. Letters 29, 650 (1972).

S.109 J. J. Wynne, Phys. Rev. B6, 534 (1972).

S.110 M. D. Levenson, C. Flytzanis, and N. Bloembergen, Phys. Rev. B6, 3462 (1972).

S.111 E. Yablonovitch, C. Flytzanis, and N. Bloembergen, Phys. Rev. Letters 29, 865 (1972).

S.112 M. D. Levenson, IEEE J. Quantum Electron. (to be published).

S.113 M. D. Levenson and N. Bloembergen (to be published).

S.114 C. Flytzanis B6, 1264 (1972).

S.115 P. R. Régnier and J. P.-E. Taran, Appl. Phys. Letters 23, 240 (1973).

S.116 N. M. Kroll, A. Ron, and N. Rostoker, Phys. Rev. Letters 13, 83 (1964); G. C. Comisar, Phys. Rev. 141, 200 (1966).

S.117 B. I. Cohen, A. N. Kaufman, K. M. Watson, Phys. Rev. Letters 29, 581 (1973).

S.118 R. A. McLaren and B. P. Stoicheff, Appl. Phys. Letters 16, 140 (1970).

S.119 S. Dumartin, B. Oksengorn, and B. Vodar, Compt. Rendus 261, 3767 (1965).

S.120 R. R. Alfano and S. L. Shapiro, Chem. Phys. Letters 8, 43 (1971).

S.121 See, for example, V. L. Strizhevskii, Sov. Phys. JETP 32, 914 (1971).

S.122 R. H. Stolen, E. P. Ippen, and A. R. Tynes, Appl. Phys. Letters 20, 62 (1972); R. H. Stolen and E. P. Ippen, Appl. Phys. Letters 22, 276 (1973).

S.123 See, for example, Ya. S. Bobovich and A. V. Bortkevich, Sov. Phys. Uspekhi 14, 1 (1971).

S.124 P. P. Sorokin, N. S. Shiren, J. R. Lankard, E. C. Hammond, E. C. Hammond, and T. G. Kazyaka, Appl. Phys. Letters 10, 44 (1967).

S.125 M. Rokni and S. Yatsiv, Phys. Letters 24A, 277 (1967); IEEE J. Quantum Electron. QE-3, 329 (1967); S. Yatsiv, M. Rokni, and S. Barak, IEEE J. Quantum Electron. QE-4, 900 (1968); S. Barak, M. Rokni, and S. Yatsiv, IEEE J. Quantum Electron. QE-5, 448 (1969); S. Barak and S. Yatsiv, Phys. Rev. A3, 382 (1971).

S.126 P. P. Sorokin, J. J. Wynne, and J. R. Lankard, Appl. Phys. Letters 22, 342 (1973).

S.127 R. T. Hodgson, P. P. Sorokin, and J. J. Wynne, Phys. Rev. Letters 32, 343 (1974).

FIGURE CAPTIONS

Fig. S.1. Schematic drawing showing the Stokes ($\omega_1 > \omega_2$) and antiStokes ($\omega_1 < \omega_2$) Raman transition from the initial state $|i\rangle$ to a final excited state $|f\rangle$.

Fig. S.2. General relationship between the wave vectors of Stokes, antiStokes, and laser waves, as stated in Eq. (S-34). (after Ref. S.22)

Fig. S.3. The Stokes power gain as a function of the normalized linear momentum mismatch $\Delta k/G_R$ in the z direction. The asymmetry is due to the nonresonant part $\chi_{NR}^{(3)} = 0.1|\mathrm{Im}\chi_R^{(3)}|_{max}$. (after Ref. S.22)

Fig. S.4. AntiStokes intensity versus the linear momentum mismatch Δk (normalized by the Stokes power gain G_R). The asymmetry is due to $\chi_{NR} = 0.1|\mathrm{Im}\chi_R^{(3)}|_{max}$. (after Ref. S.22)

Fig. S.5. The saturation effect of a single-mode laser beam of infinite extent. The intensities of the various orders of Stokes waves are normalized by the incoming laser intensity. The distance is also normalized to a dimensionless one $Z = (16\pi^3\omega_1^2\mathrm{Im}\chi_R/C^3k_1)P_1(0)z$. (after Ref. S.22)

Fig. S.6. A typical experimental setup for investigation of stimulated Raman scattering. PM1, PM2, and PM3 are photo-detectors measuring the laser, the forward Raman, and the backward Raman radiation respectively.

Fig. S.7. First-order forward and backward Stokes power versus the toluene cell length at three laser powers $P_1 = 80$, $P_2 = 67$, and $P_3 = 53$ MW/cm^2. (after Y. R. Shen and Y. J. Shaham, Phys. Rev. 163, 224 (1967)).

Fig. S.8. Comparison of experimental data (Ref. S.55) and theoretical curve (Ref. S.25) of first-order Stokes power as a function of incident laser power in liquid nitrogen.

Fig. S.9. Experimental setup for measuring backward Stokes gain. (after Ref. S.57)

Fig. S.10. Stokes Raman gain in H_2 gas as a function of pressure. The data points X for forward gain should be compared with the dashed theoretical curve (cell length, 80 cm; peak input intensity 20 MW/cm^2). The data points + for backward gain should be compared with the solid theoretical curve (cell length, 30 cm; peak input intensity, 60 MW/cm^2). (after Ref. S.57)

Fig. S.11. Multicolor antiStokes rings created in benzene by a ruby laser beam. (after A. Yariv, Quantum Electronics (John Wiley, Inc., New York, 1967)) (picture taken by R. W. Terhune).

Fig. S.12. Normalized transmitted laser (R_L), first (R_{S1}) and second Stokes (R_{S2}) power as a function of the incident laser intensity $I_L(0,0)$. The experimental data of R_L, R_{S1}, and R_{S2} are represented by circles, rectangles, and diamonds respectively. The curves are calculated according to the theory in Section S.2.5 with the finite beam cross-section taken into account. (after Ref. S.42)

Fig. S.13. (a) Relative parametric gain $(g_2)_{max}$ versus the idler frequency ω_1 for gallium phosphide. Solid portion of the curve indicates the frequency range of the idler over which phase matching is possible. (b) Infrared absorption coefficient for gallium phosphide using $\Gamma = 4\ cm^{-1}$ (c) Ratio of the idler flux density S_1 to the signal flux density S_2. (after Ref. S.63)

Fig. S.14. Plots of stimulated gain coefficient (g_s) as a function of idler frequency for the 248 cm^{-1} mode (Curve a) and the 628 cm^{-1} mode (Curve b). (after Ref. S.66)

Fig. S.15. Schematic of spin-flip Raman process in n-InSb.

Fig. S.16. Resonance enhancement of spontaneous spin-flip Raman scattering as a function of input photon energy. $n = 1 \times 10^{16}$ cm^{-3}, H = 40 kG, and T ~ 30°K. (after Ref. S.72)

Fig. S.17. Theoretical curves of the Raman gain g, and the ratios of the far-infrared output $P(\omega_3)$ to the Raman output $P(\omega_2)$ for the collinear phase-mismatched case and for the noncollinear phase-matched case. (see Ref. S.16)

Fig. S.18. Calculated normalized Raman pulse intensity as a function of time for an initial condition $|E_s| = |E_{so}|(t - t_o)^3$ for $t > t_o$. The curves show the pulse development at length intervals of $\Delta\ell = 2.77/G$. G is the Raman gain and was determined to be 0.7 cm^{-1} in CS_2. Lower scale is in dimensionless units; upper scale describes the experimental conditions. (after Ref. S.50)

Fig. S.19. The transient Raman gain coefficient for Gaussian laser input pulses with the same total energy, but different pulse widths. The steady state gain coefficient G_{SS} corresponds to a constant intensity laser output equal to the maximum laser pulse intensity. (after Ref. S.91)

Fig. S.20. The variation of Stokes pulse width t_S and delay t_D with transient gain coefficient, for Gaussian laser input pulses of various widths t_p given in terms of the optical phonon dephasing time Γ^{-1}. (after Ref. S.91)

Fig. S.21. Schematic of the experimental system for phonon lifetime measurement. The pump beam B1 at $\lambda \simeq 1.06\mu m$ and the probe beam B2 at $\lambda \simeq 0.53\mu m$ interact in the Raman sample RS. Glass rod for fixed optical delay, FD; glass prisms for variable delay, VD; filter, F;

photodetector, P; two-photon-fluorescence system, TPF. (after Ref. S.104)

Fig. S.22. Measured incoherent scattering $S^{inc}(t_D)/S_{max}{}^{inc}$ (closed circles) and coherent scattering $S^{coh}(t_D)/S_{max}{}^{coh}$ (open circles) versus delay time t_D for ethyl alcohol. The solid and dashed curves are calculated./ (after Ref. S.104)

Fig. S.23. Typical results for the/intensity at ω_3 in calcite. The antiStokes polarizations were perpendicular to the optic axis of calcite. (after Ref. S.112

Fig. S.24. The nonlinear spectroscopy system. The output of laser 1 is shown as a dashed line, that of laser 2 as a dotted line. Both laser beams are blocked after the samples, and the output due to frequency mixing is collected and directed into the monochromators. (after Ref. S.112)

TABLE CAPTIONS

Table S.1. Frequency shift, linewidth, and scattering cross-section of spontaneous Raman scattering for a number of substances and the corresponding stimulated Raman gain.

Table S.2. Observed stimulated Raman lines in a number of crystals.

Substance	Raman Shift (cm^{-1})	Linewidth 2Γ (cm^{-1})	Cross-section $d\sigma/d\Omega \times 10^8$ (cm^{-1}-$ster^{-1}$)	Raman Gain $G_R \times 10^3$ (cm/MW)
Gas H_2†	4155	0.2		1.5 (300°K, 10 atm.)
Liquid O_2	1522	0.177	0.48 ± 0.14	14.5 ± 4
Liquid N_2	2326.5	0.067	0.29 ± 0.09	17 ± 5
Benzene	992	2.15	3.06	2.8
CS_2	655.6	0.50	7.55	24
Nitrobenzene	1345	6.6	6.4	2.1
$LiNbO_3$	258	7	262	28.7
InSb*	0 - 300	0.3	10	1.7×10^4

† E. E. Hagenlocker, R. W. Minck, and W. G. Rado, Phys. Rev. 154, 226 (1967).

* For a carrier concentration $n_e \simeq 10^{16}$ cm^{-3}.

Table S.1

Crystal	Stimulated Raman Shift (cm^{-1})	References
$CaCO_3$	1086	a
Si	521	b
Diamond	1332	a
InSb	0 - 300	c
$LiNbO_3$	42 - 200	d
α-sulfur	216, 470	a
$CaWO_4$	911	a

a G. Eckardt, IEEE J. Quantum Electron. 2, 1 (1966).

b J. M. Ralston and R. K. Chang, Phys. Rev. B2, 1858 (1970).

c C. K. N. Patel and E. D. Shaw, Phys. Rev. B3, 1279 (1971).

d J. Gelbwachs, R. H. Pantell, H. E. Puthoff, and J. M. Yarborough, Appl. Phys. Letters 14, 258 (1969).

Table S.2

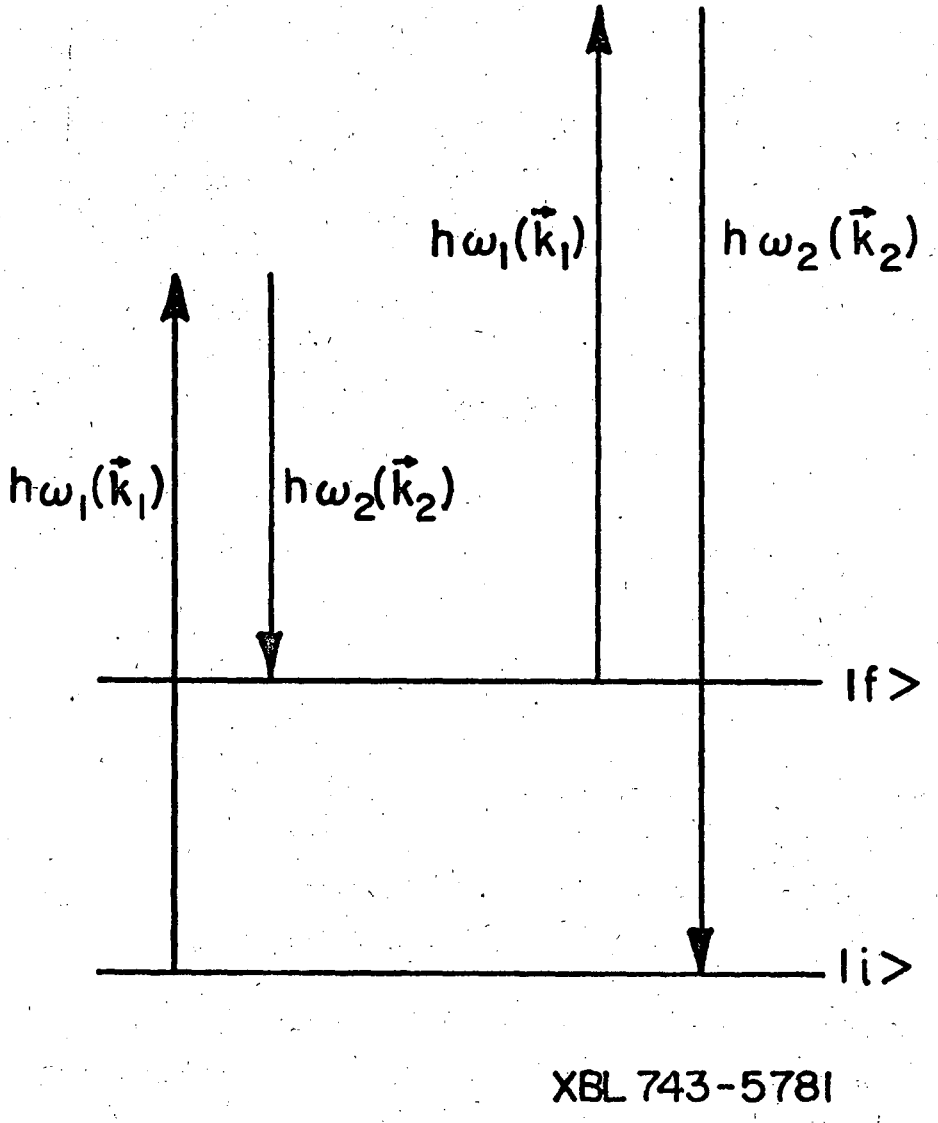
$\hbar\omega_1(\vec{k}_1)$
$\hbar\omega_2(\vec{k}_2)$
$\hbar\omega_1(\vec{k}_1)$
$\hbar\omega_2(\vec{k}_2)$
|f>
|i>
XBL 743-5781

Fig. 1

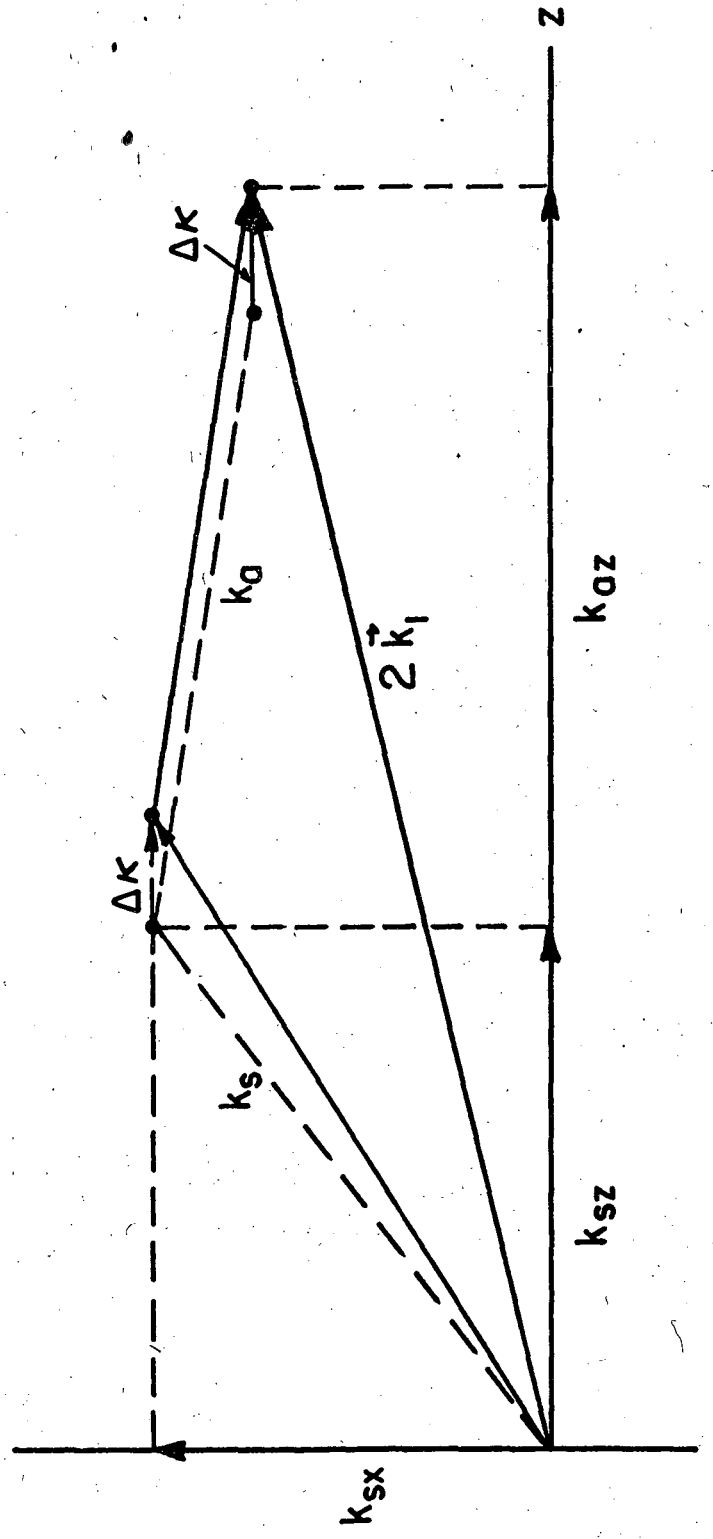

XBL 743-5782

Fig. 2

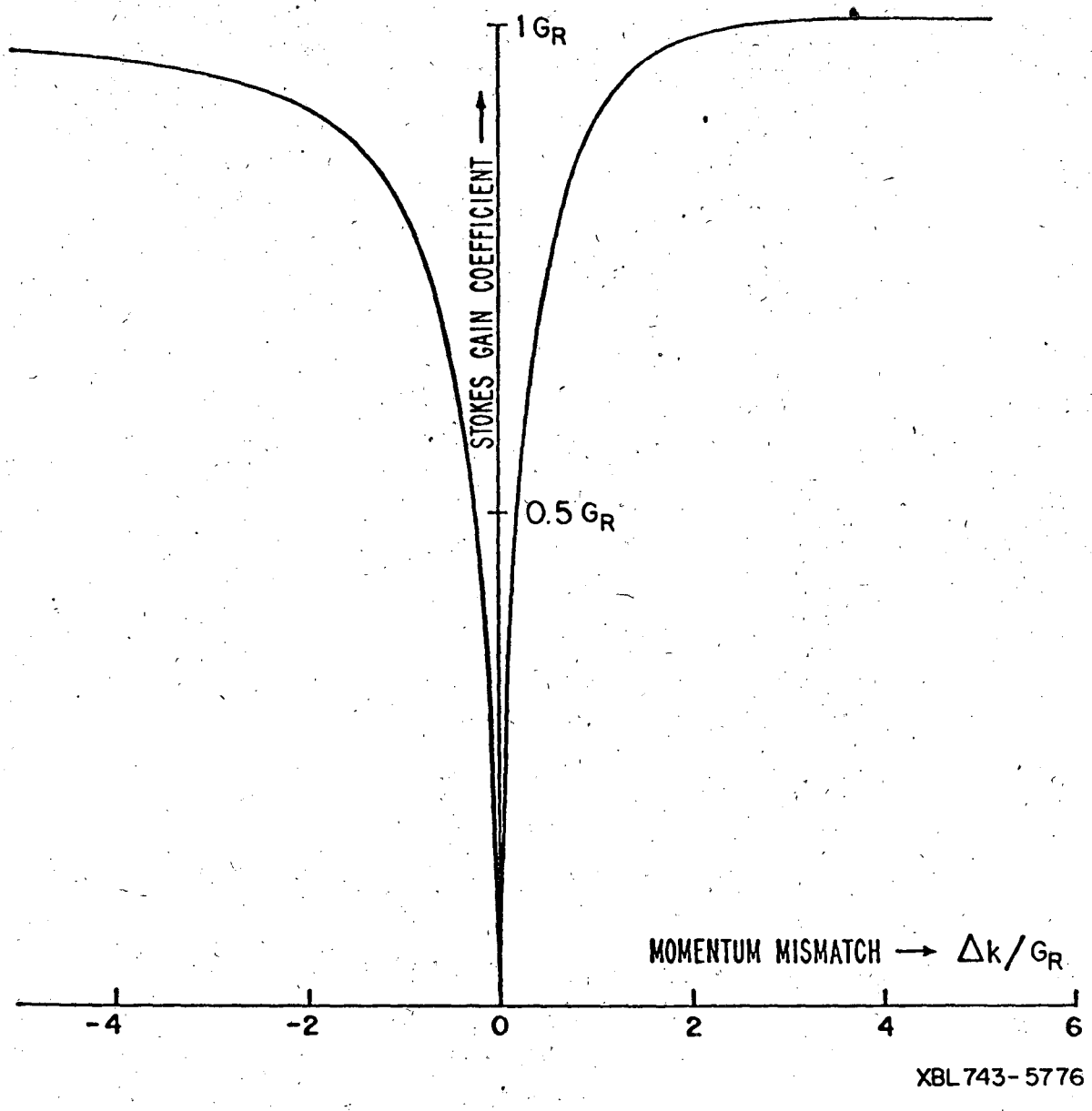
1 G_R
STOKES GAIN COEFFICIENT
0.5 G_R
MOMENTUM MISMATCH → $\Delta k / G_R$
-4
-2
0
2
4
6
XBL743-5776

Fig. 3

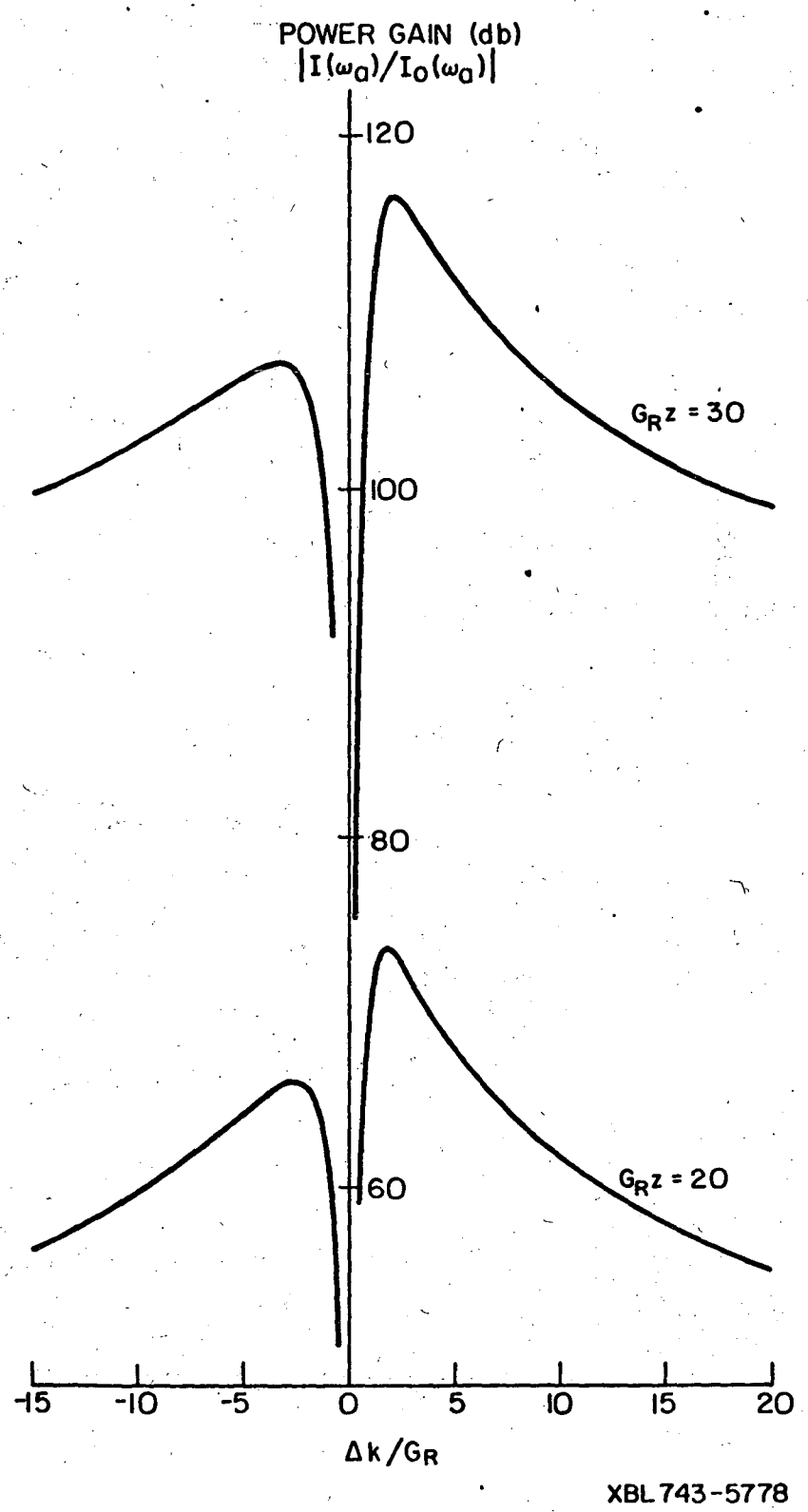
POWER GAIN (db)
$|I(\omega_a)/I_0(\omega_a)|$
120
100
80
60
$G_R z = 30$
$G_R z = 20$
-15
-10
-5
0
5
10
15
20
$\Delta k/G_R$
XBL743-5778

Fig. 4

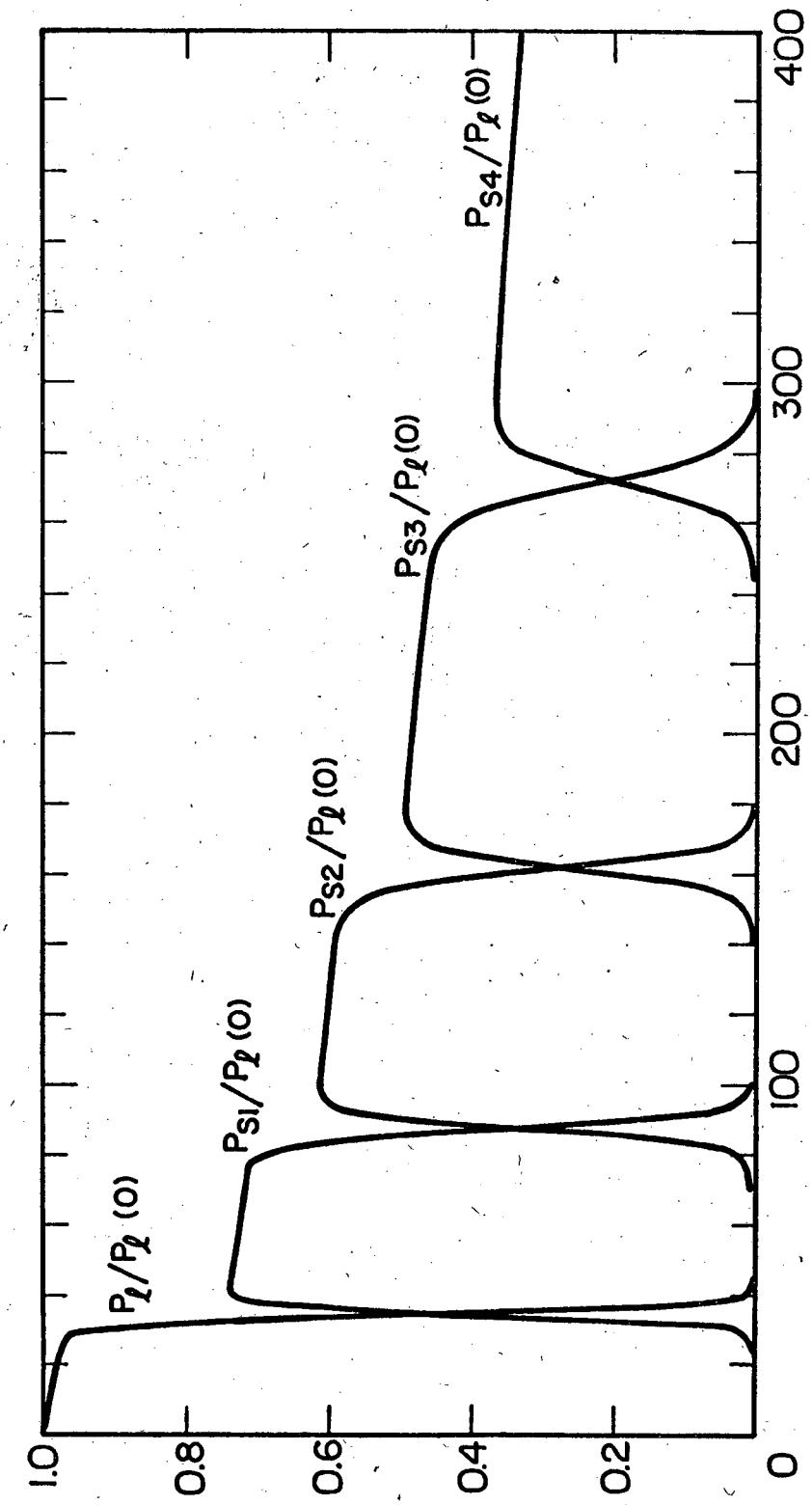
1.0
0.8
0.6
0.4
0.2
0
100
200
300
400
Z
$P_{\ell}/P_{\ell}(0)$
$P_{S1}/P_{\ell}(0)$
$P_{S2}/P_{\ell}(0)$
$P_{S3}/P_{\ell}(0)$
$P_{S4}/P_{\ell}(0)$
XBL743-5777

Fig. 5

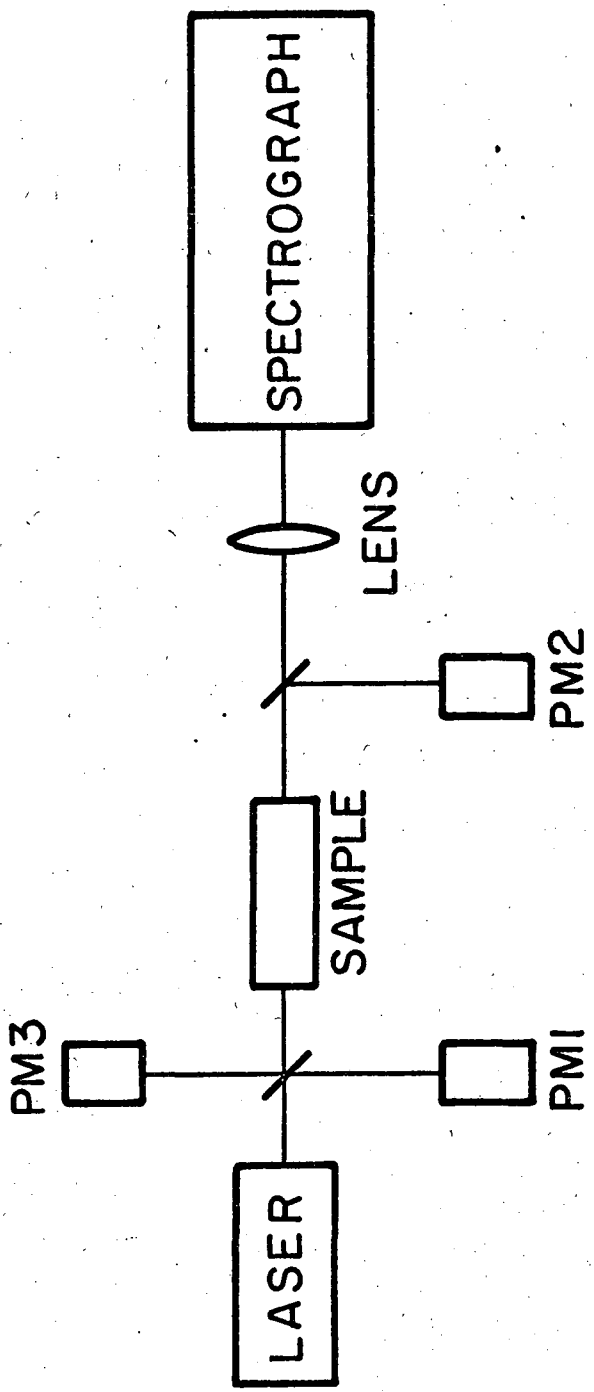

Fig. 6

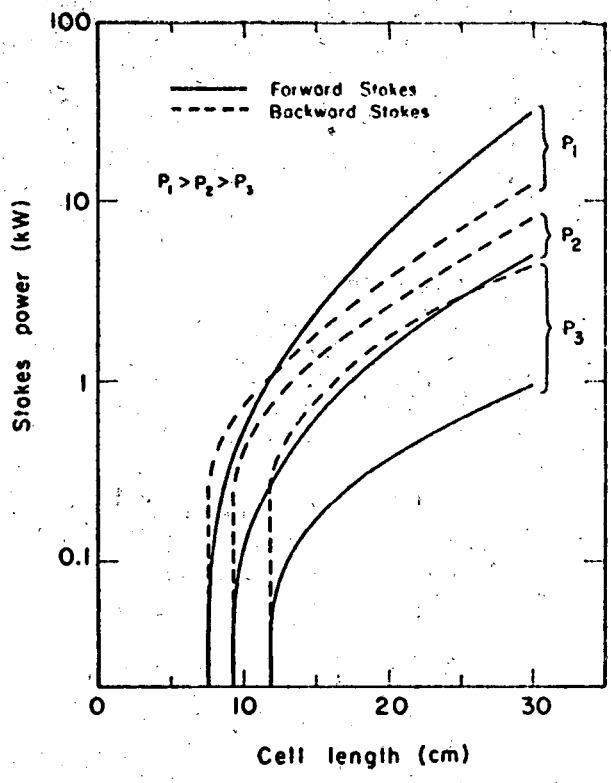

XBL 743-5794

Fig. 7

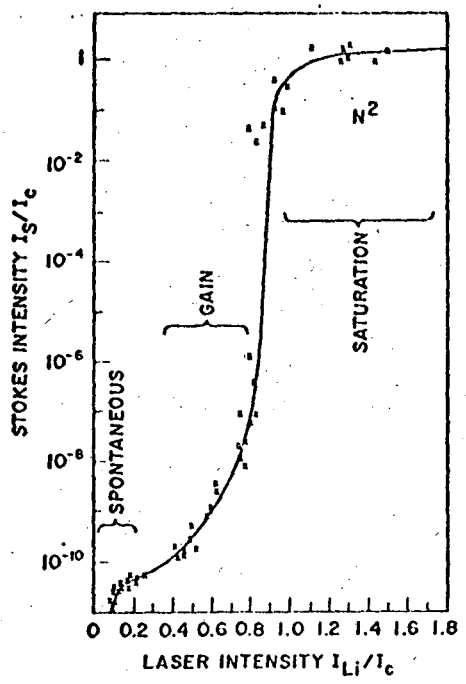
STOKES INTENSITY I_S/I_c
1
10^{-2}
10^{-4}
10^{-6}
10^{-8}
10^{-10}
N^2
GAIN
SATURATION
SPONTANEOUS
0 0.2 0.4 0.6 0.8 1.0 1.2 1.4 1.6 1.8
LASER INTENSITY I_{Li}/I_c

Fig. 8

Fig. 8

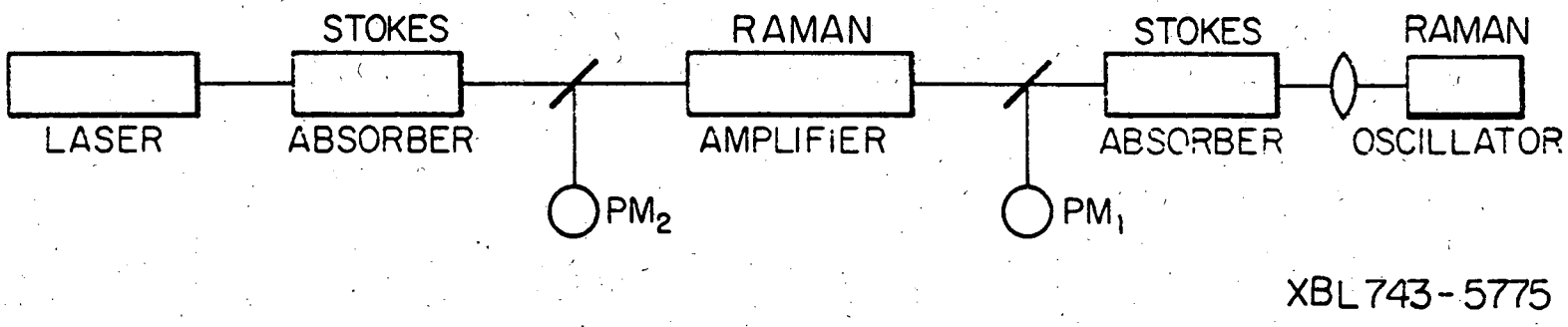
STOKES
RAMAN
STOKES
RAMAN
LASER
ABSORBER
AMPLIFIER
ABSORBER
OSCILLATOR
PM2
PM1
XBL743-5775

Fig. 9

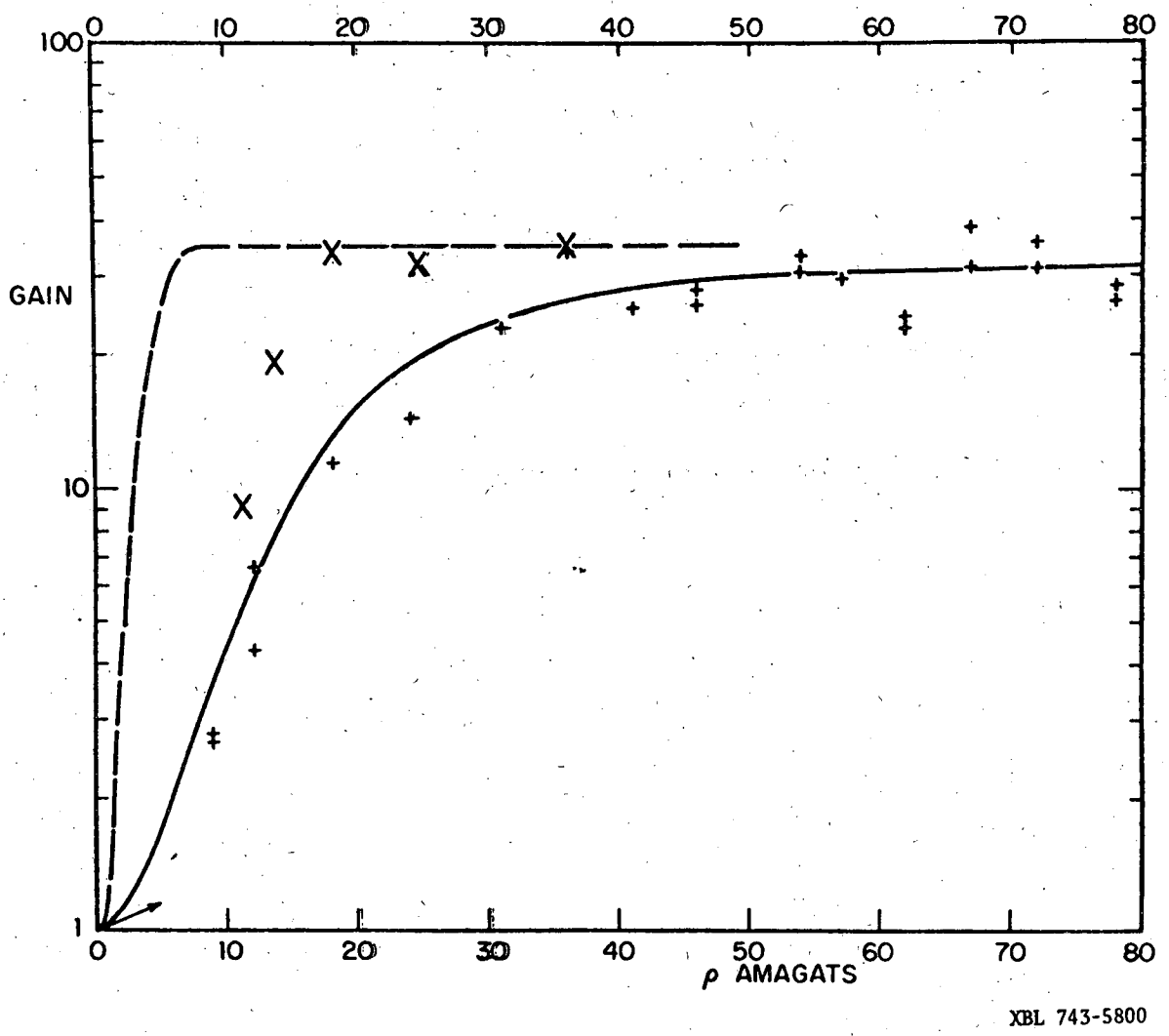

Fig. 10

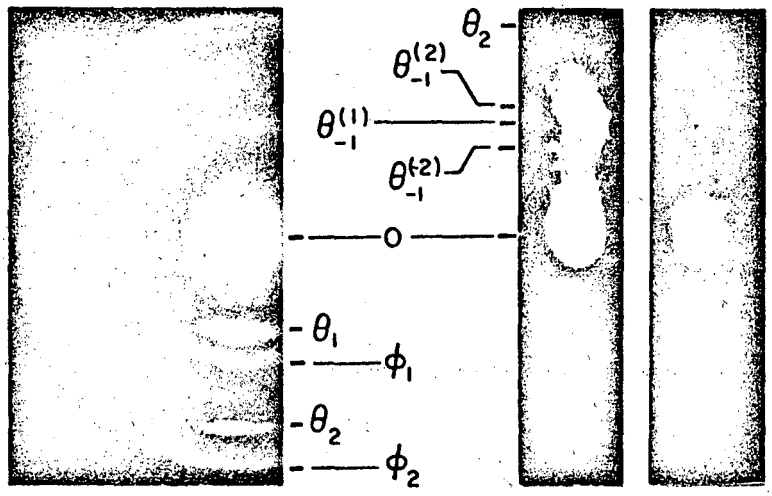
θ_2
$\theta_{-1}^{(2)}$
$\theta_{-1}^{(1)}$
$\theta_{-1}^{(2)}$
0
θ_1
ϕ_1
θ_2
ϕ_2
(a)
(b)

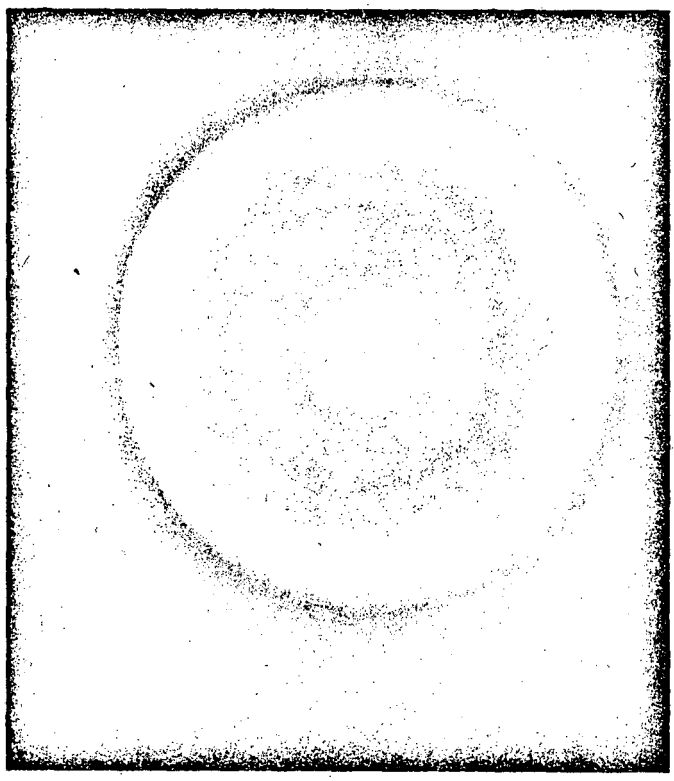

Fig. 11

Fig. 11

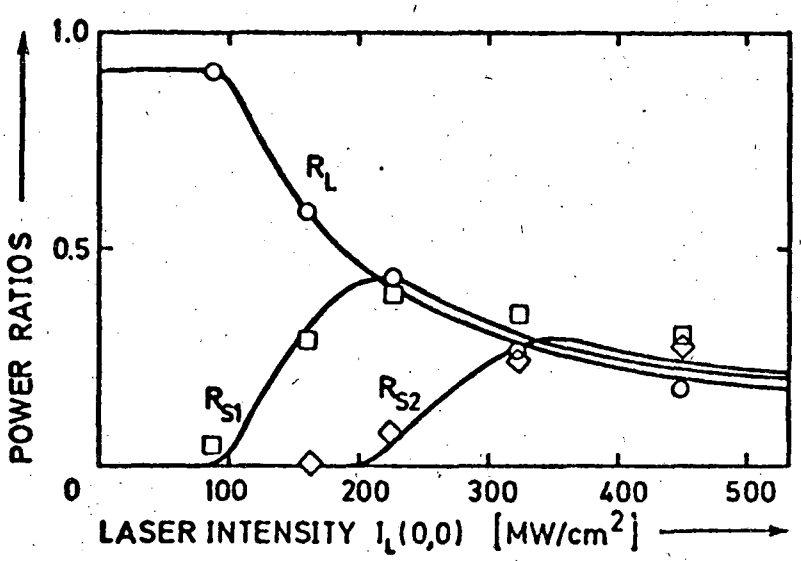

XBL 743-5798

Fig. 12

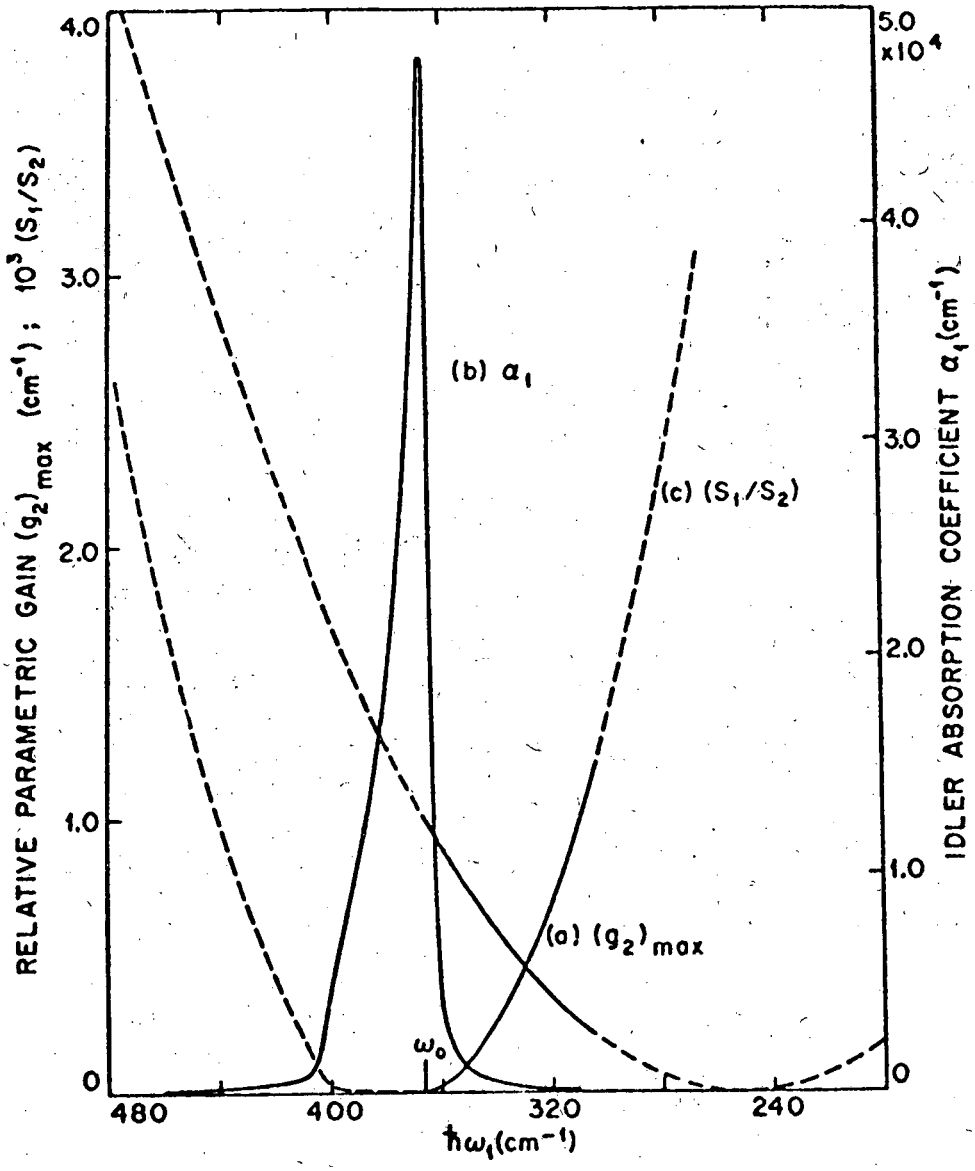

XBL 743-5799

Fig. 13

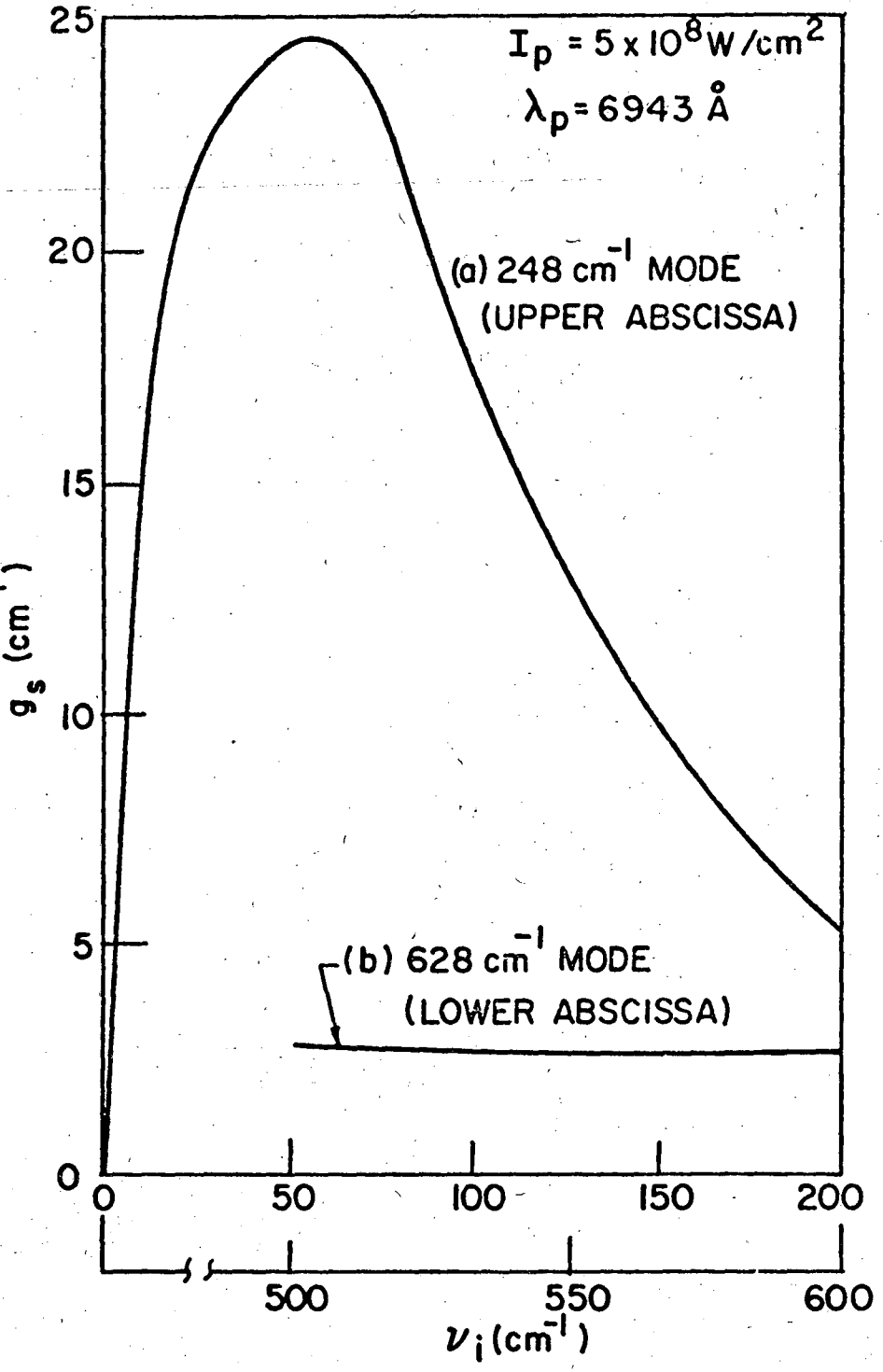

XBL 743-5807

Fig. 14

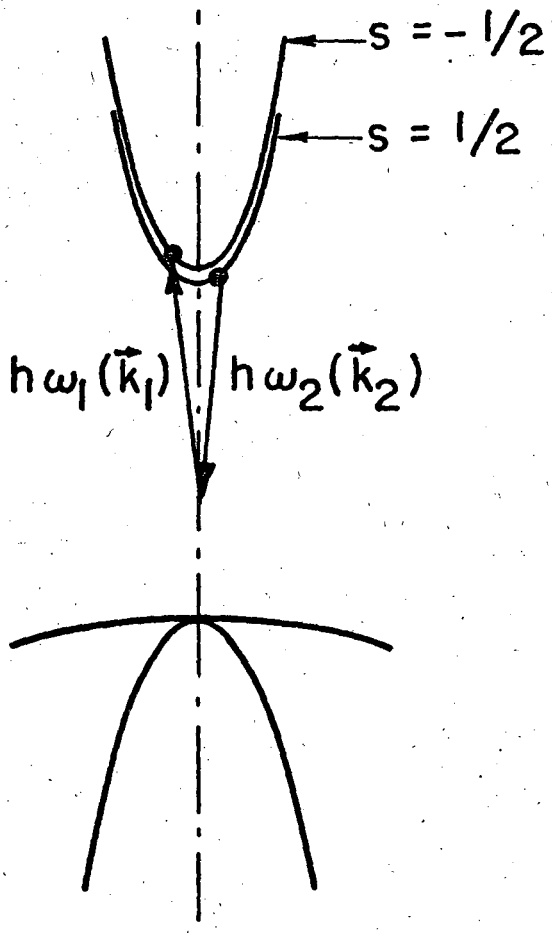

XBL743-5779

Fig. 15

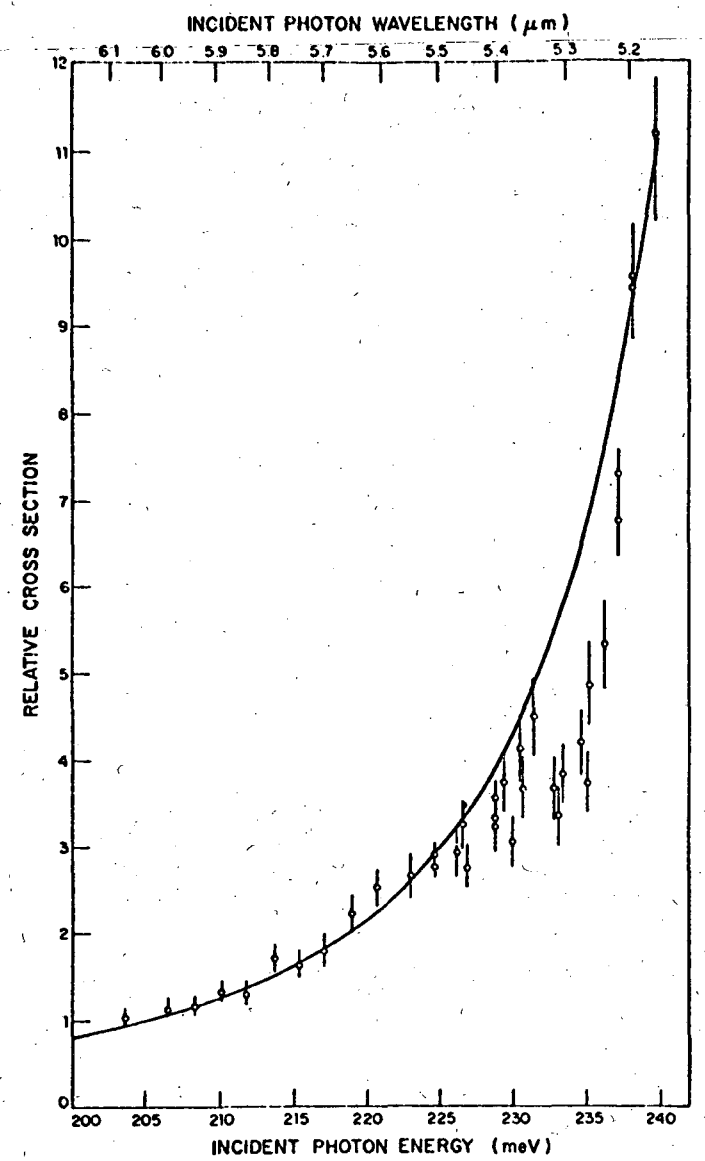

XBL 743-5802

Fig. 16

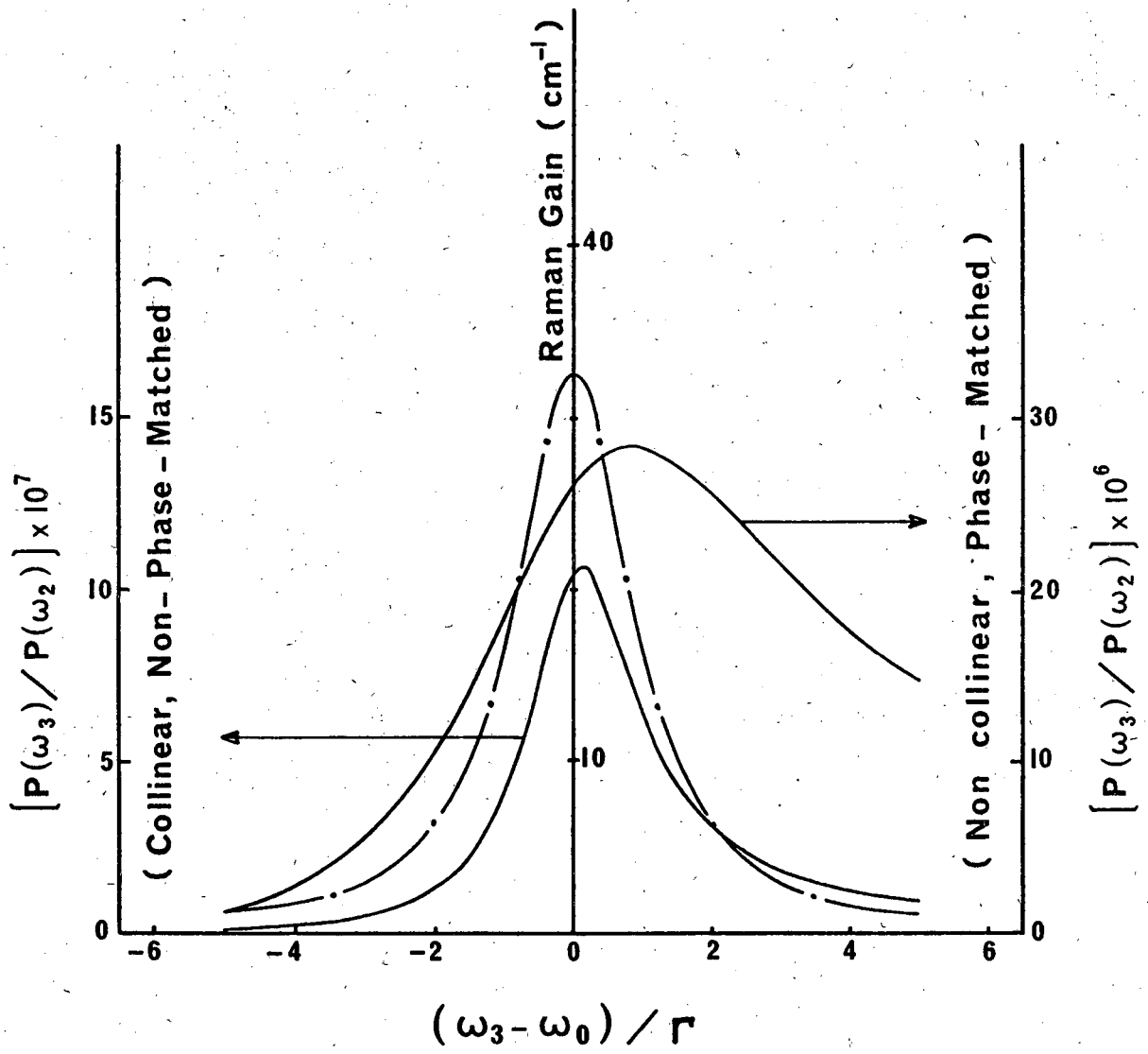

XBL 743-5795

Fig. 17

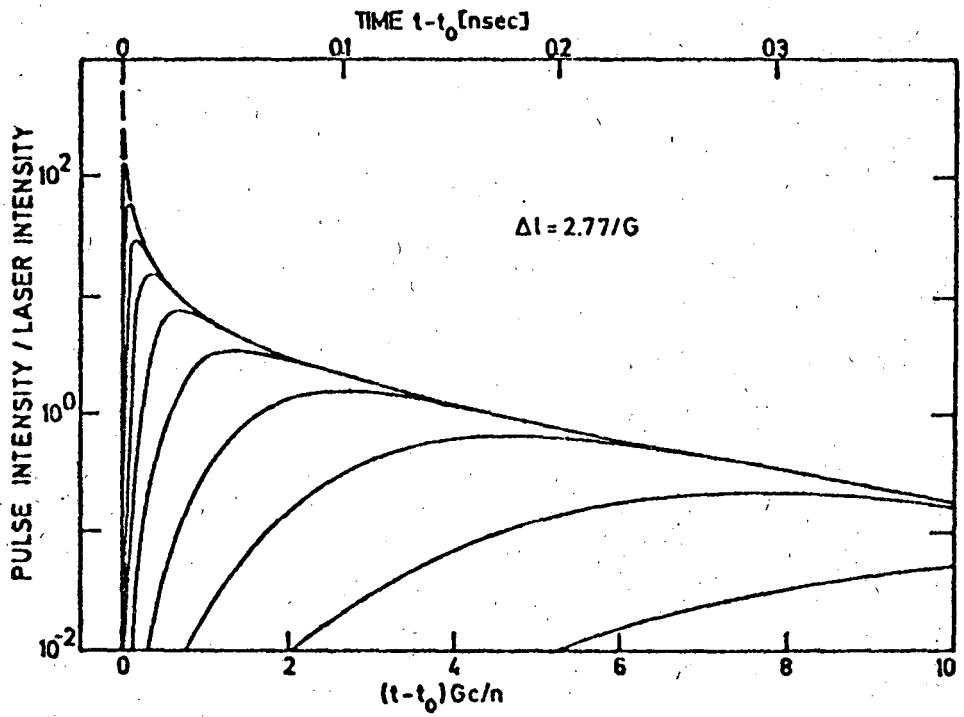

XBL 743-5808

Fig. 18

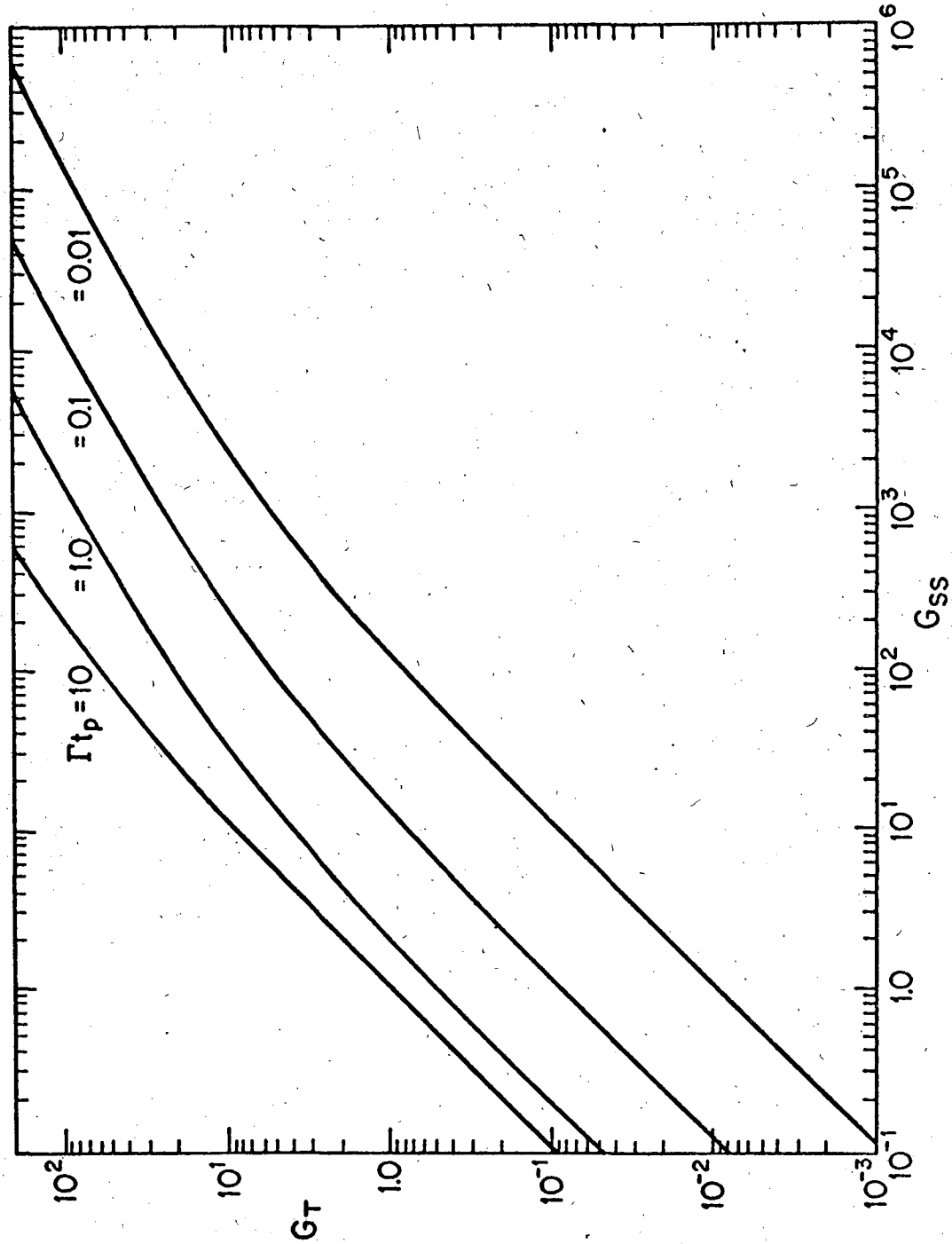

XBL 743-5803

Fig. 19

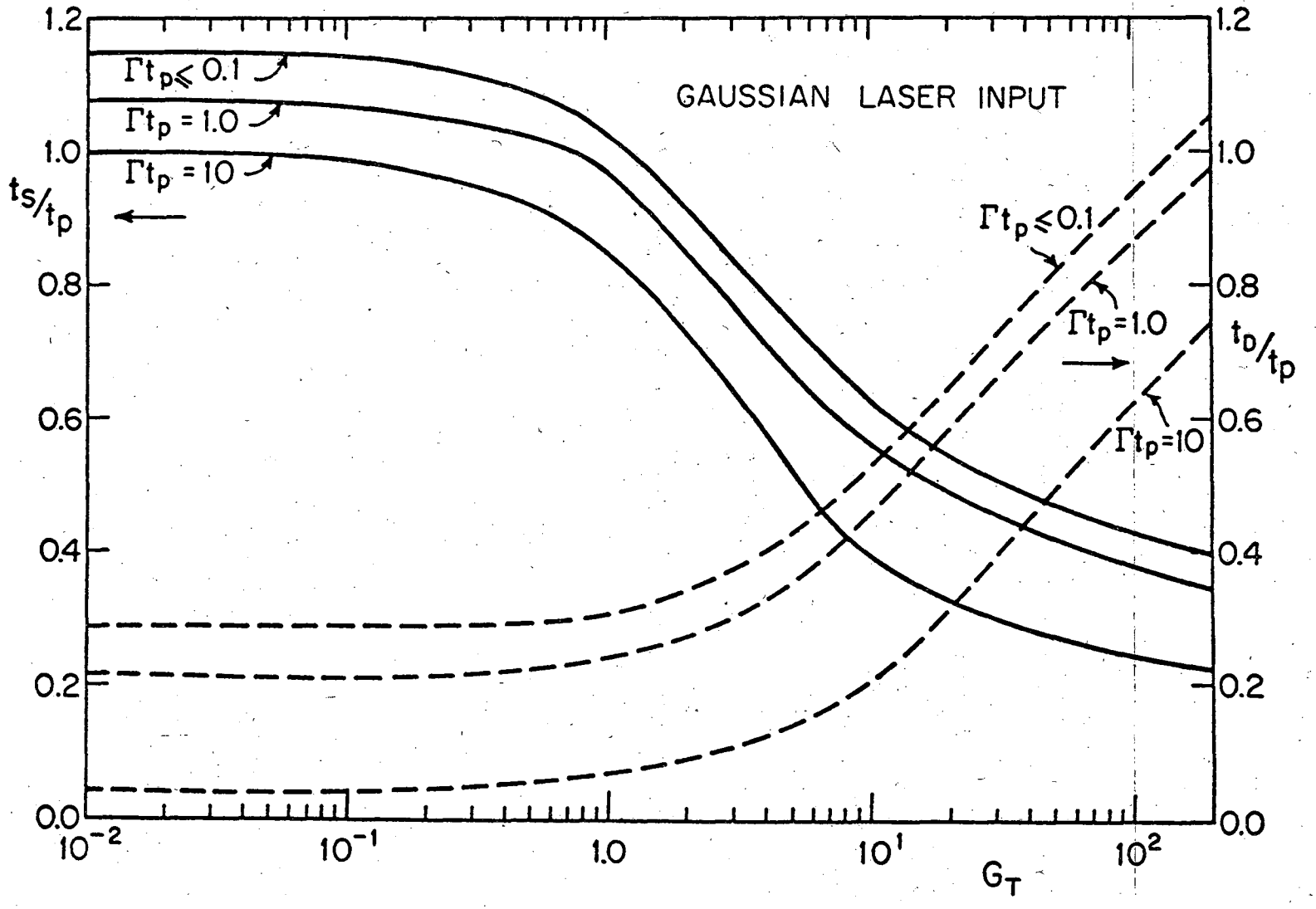

XBL 743-5801

Fig. 20

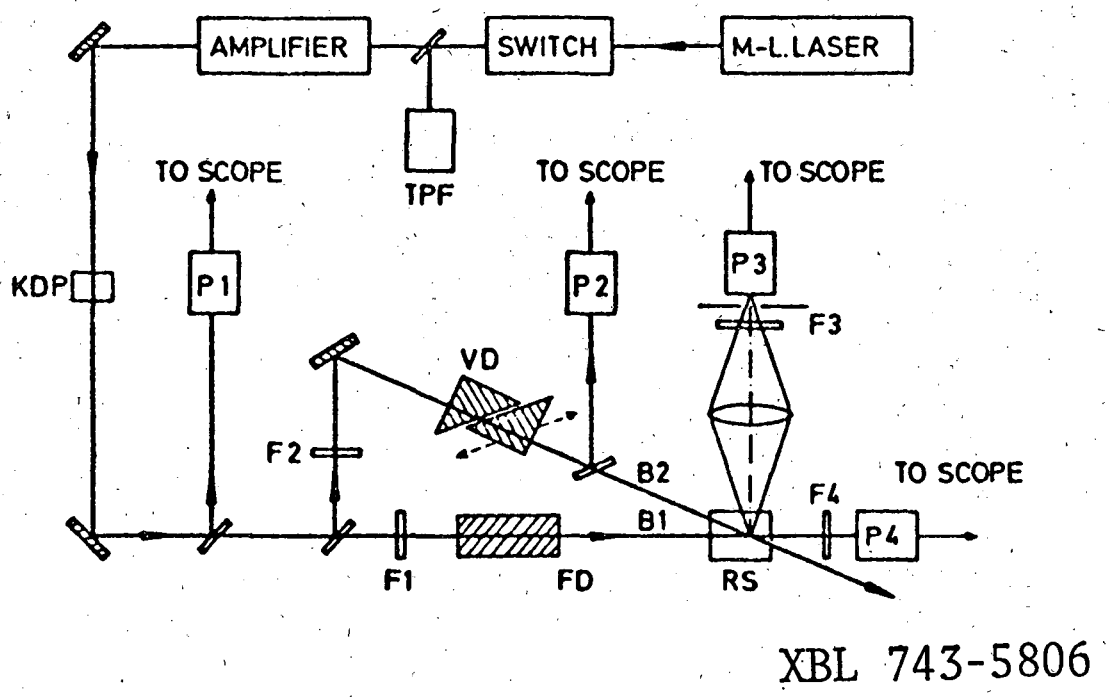
AMPLIFIER
SWITCH
M-L.LASER
TPF
TO SCOPE
TO SCOPE
TO SCOPE
KDP
P1
P2
P3
F3
VD
F2
B2
F4
TO SCOPE
B1
P4
F1
FD
RS
XBL 743-5806

Fig. 21

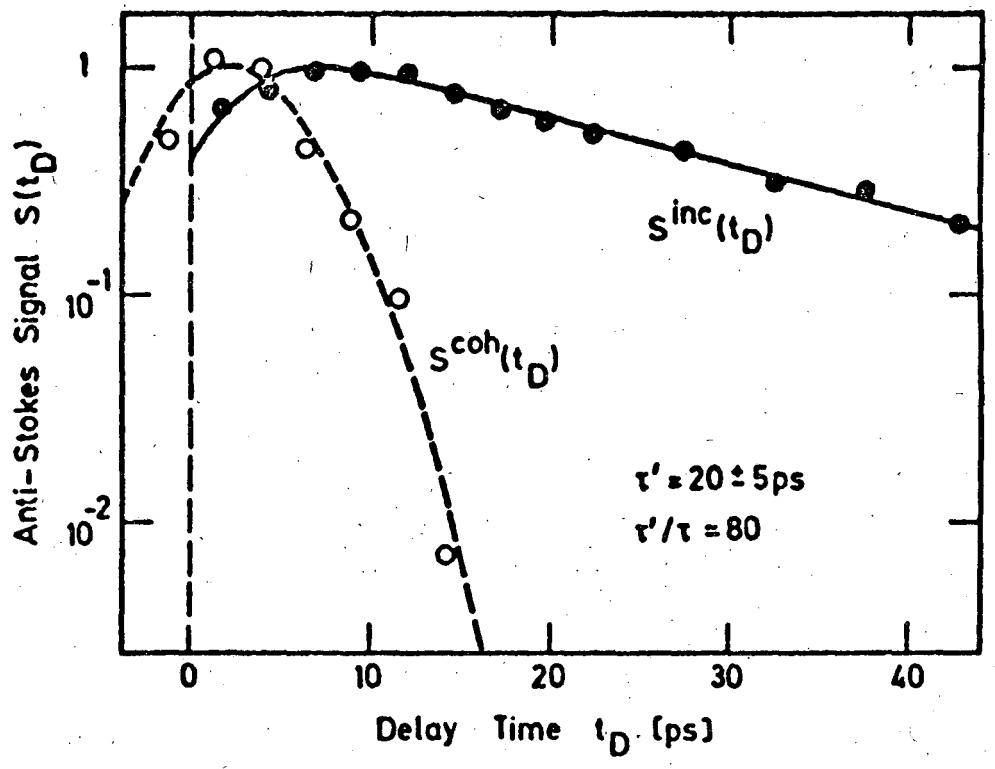

XBL 743-5805

Fig. 22

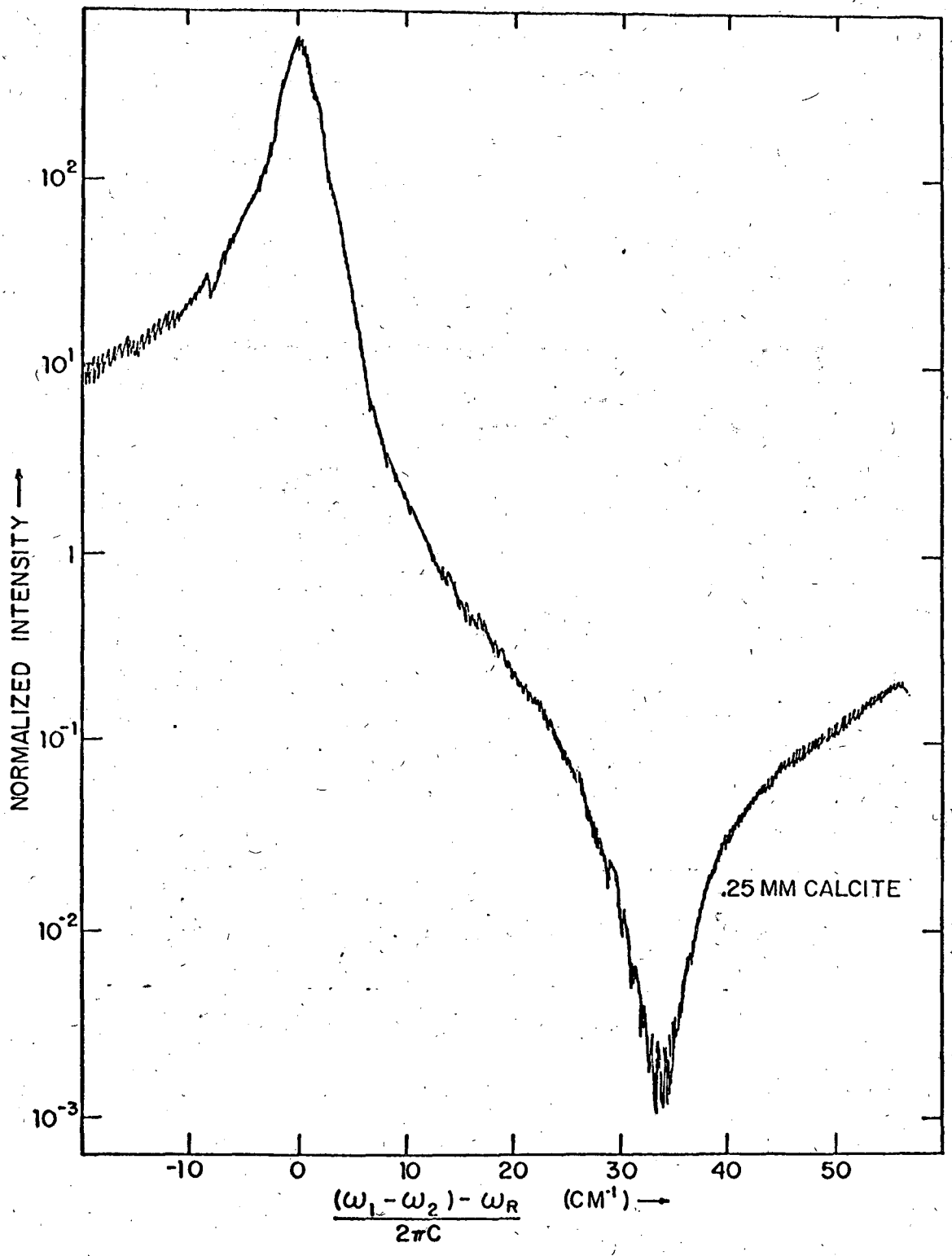
NORMALIZED INTENSITY
10^2
10^1
1
10^{-1}
10^{-2}
10^{-3}
-10
0
10
20
30
40
50
$\frac{(\omega_1 - \omega_2) - \omega_R}{2\pi C}$ (CM^{-1})
.25 MM CALCITE
XBL 743-5809

Fig. 23

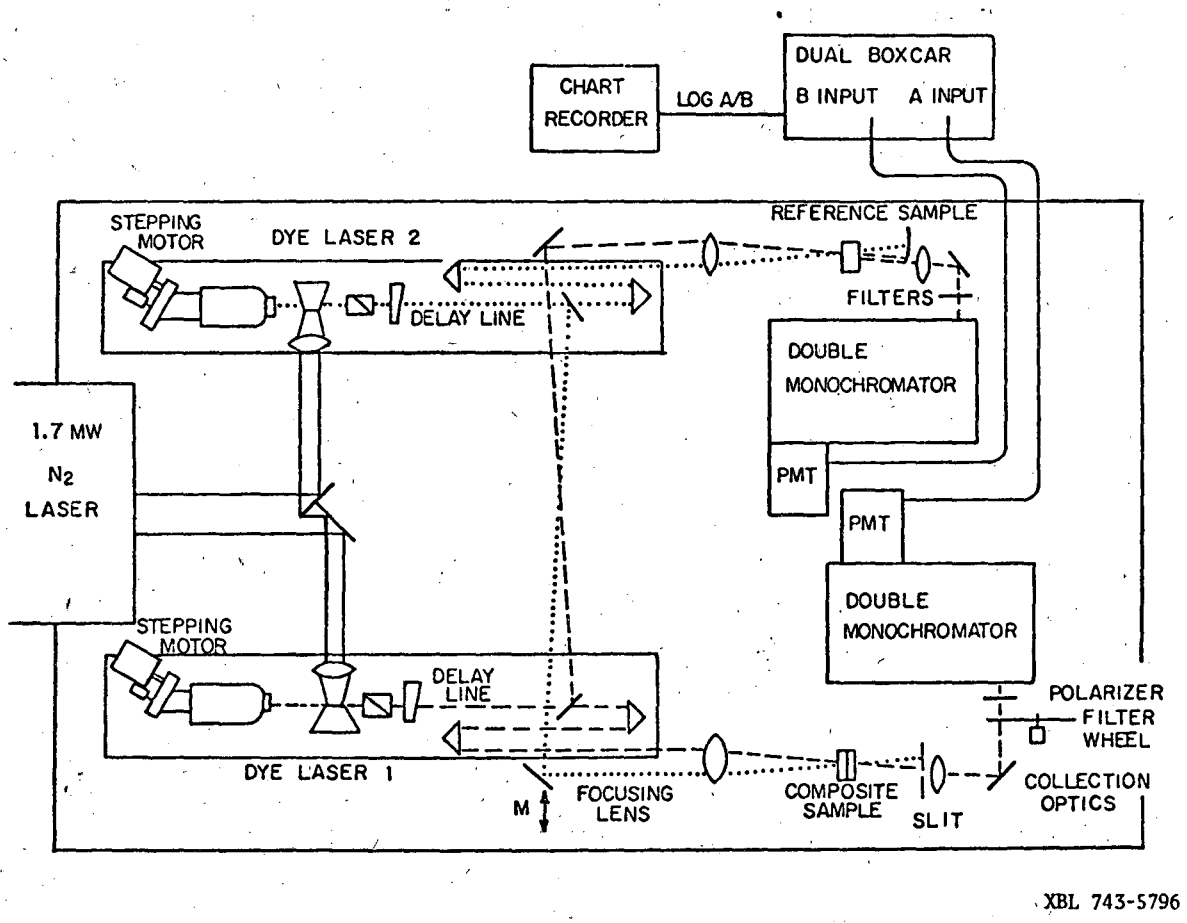
CHART RECORDER
LOG A/B
DUAL BOXCAR
B INPUT
A INPUT
STEPPING MOTOR
DYE LASER 2
DELAY LINE
REFERENCE SAMPLE
FILTERS
DOUBLE MONOCHROMATOR
PMT
PMT
DOUBLE MONOCHROMATOR
1.7 MW
N_2
LASER
STEPPING MOTOR
DELAY LINE
DYE LASER 1
POLARIZER
FILTER WHEEL
COLLECTION OPTICS
M
FOCUSING LENS
COMPOSITE SAMPLE
SLIT
XBL 743-5796

Fig. 24

TECHNICAL INFORMATION DIVISION
LAWRENCE BERKELEY LABORATORY
UNIVERSITY OF CALIFORNIA
BERKELEY, CALIFORNIA 94720